scientific reports

Check for updates

OPEN

The PaleoJump database for abrupt transitions in past climates

Witold Bagniewski[1]✉, Denis-Didier Rousseau[2,3,4] & Michael Ghil[1,5]

Tipping points (TPs) in Earth's climate system have been the subject of increasing interest and concern in recent years, given the risk that anthropogenic forcing could cause abrupt, potentially irreversible, climate transitions. Paleoclimate records are essential for identifying past TPs and for gaining a thorough understanding of the underlying nonlinearities and bifurcation mechanisms. However, the quality, resolution, and reliability of these records can vary, making it important to carefully select the ones that provide the most accurate representation of past climates. Moreover, as paleoclimate time series vary in their origin, time spans, and periodicities, an objective, automated methodology is crucial for identifying and comparing TPs. To address these challenges, we introduce the open-source PaleoJump database, which contains a collection of carefully selected, high-resolution records originating in ice cores, marine sediments, speleothems, terrestrial records, and lake sediments. These records describe climate variability on centennial, millennial and longer time scales and cover all the continents and ocean basins. We provide an overview of their spatial distribution and discuss the gaps in coverage. Our statistical methodology includes an augmented Kolmogorov–Smirnov test and Recurrence Quantification Analysis; it is applied here, for illustration purposes, to selected records in which abrupt transitions are automatically detected and the presence of potential tipping elements is investigated. These transitions are shown in the PaleoJump database along with other essential information about the records, including location, temporal scale and resolution, as well as temporal plots. This open-source database represents, therefore, a valuable resource for researchers investigating TPs in past climates.

Since the discovery of Dansgaard-Oeschger (DO) events in Greenland ice cores[1–3], climate research has aimed to identify other examples of centennial-to-millennial climate variability, including in marine and terrestrial paleoclimate records[4,5], and to gain insight into the mechanisms behind these changes. Many such records exhibit abrupt transitions, raising the question of whether similarly drastic changes may occur in the near future, as anthropogenic global warming pushes the climate system away from the relatively stable state that has persisted throughout the Holocene. Many of Earth's subsystems exhibit intrinsic variability and respond nonlinearly to various natural and anthropogenic forcings[6,7]. Hence, any of these subsystems could experience a sudden shift into a new state once certain key thresholds, known as tipping points (TPs), are crossed[8–10].

Identifying potential TPs in the climate system requires theoretical and modeling work, including comparison with observations. Proxy records of past climate and environmental changes play a crucial role, by enabling the reconstruction of Earth's climatic history. These records, particularly those that show abrupt transitions, may provide valuable insights into the past behavior of Earth's systems and possible TPs. By using this information, we can gain a better understanding of the possible trajectories of future climate change and their environmental impacts.

With tens of thousands of paleoclimate datasets available, finding and selecting the most relevant records for studying past climate can be overwhelming. These proxy datasets originate from different geologic structures, contain different variables, and span a wide range of age intervals with different resolutions. In addition, due to the varying resolution and dating methods used for these records, it is important to assess their reliability. There have been efforts in recent years to build compilations of high-quality paleoclimate data, such as the ACER database of pollen and charcoal records from the last glacial period[11], the SISAL database of speleothem isotope

[1]Department of Geosciences and Laboratoire de Météorologie Dynamique (CNRS and IPSL), École Normale Supérieure, PSL University, Paris, France. [2]Geosciences Montpellier, CNRS, University of Montpellier, Montpellier, France. [3]Institute of Physics - CSE, Division of Geochronology and Environmental Isotopes, Silesian University of Technology, Gliwice, Poland. [4]Lamont-Doherty Earth Observatory, Columbia University, New York, USA. [5]Department of Atmospheric and Oceanic Sciences, University of California at Los Angeles, Los Angeles, USA. ✉email: wbagniewski@lmd.ipsl.fr

records[12], the PalMod compilation of marine sediment data covering the last glacial-interglacial cycle[13], the World Atlas of late Quaternary Foraminiferal Oxygen and Carbon Isotope Ratios[14], and the PhanSST database of Phanerozoic sea surface temperature proxy data[15]. These compilations, however, are typically limited to a specific type of proxy or time interval.

To fully understand TPs, which can affect various components of the earth system[6,9,16] and have occurred at different times in the past, it is essential to examine a diverse range of paleoclimate data. This includes marine, terrestrial, and ice records from different time intervals during which abrupt climate change events have occurred, such as the Paleocene-Eocene Thermal Maximum (PETM), DO events, and the Younger Dryas. Furthermore, as tipping elements—the subsystems that may be subject to tipping—are interconnected, a potential for domino effects exists[17]. To identify and describe such effects in past records, one needs coverage from different types of archives with a comprehensive geospatial distribution.

The purpose of this paper is to address these challenges by presenting the open-source PaleoJump database[18], https://paleojump.github.io, which compiles globally sourced high-resolution paleoclimate records that contain abrupt transitions. The records originate in ice cores, marine sediments, speleothems, terrestrial deposits, and lake sediments, and can provide valuable information for modeling and predicting critical TPs in current and future climate evolution. The database is designed as a website, allowing easy access and navigation. It includes a map of the paleoclimate records, as well as tables that list supplementary information for each record, along with dates of the detected transitions.

In addition to providing a description of the PaleoJump database, we demonstrate its potential use by conducting a TP analysis of seven records selected from the database. Since paleoclimate records vary in their origin, time spans, and periodicities, an objective, automated methodology is key for identifying and comparing TPs. Here, we apply a recently developed method to detect abrupt transitions based on an augmented Kolmogorov–Smirnov (KS) test[19] to the selected records. The KS test results are then compared with those of recurrence quantification analysis (RQA)[20,21] to further assess the validity of the findings.

The next section describes the database itself, followed by a section summarizing the KS and RQA methods. Next, a section illustrates the application of these two methods to the seven selected records, including comparisons between the results for distinct records. The following section compares the results of the two methods and provides an interpretation of our findings. Conclusions of the work follow in the last section.

Database sources

The PaleoJump database currently includes records from 131 sites, grouped by their geological type: 49 marine-sediment cores, 32 speleothems, 18 lake sediment cores, 20 terrestrial records, and 12 ice cores. The main sources for this database are the PANGAEA and NCEI/NOAA open-access data repositories, while some records are, unfortunately, available only on request from the authors of the original studies; in the latter case, links to the corresponding articles are provided. The paleorecords have been selected for their ability to represent different aspects of past climate and environmental variability. In addition to containing abrupt transitions, these records are characterized by high temporal resolution, multi-millennial time scales, and a comprehensive spatial coverage. This selection simplifies the search for records that are most helpful in the investigation of critical transitions and of the behavior of tipping elements.

Resolution is a crucial factor in the selection of records. As a metric, we use 'maximum resolution', which we define as the temporal resolution of the 10 ky interval with the smallest average time step. We took this approach to ensure that records with nonuniform resolution or with gaps in the data are not overlooked. To make the selection more conservative, we only considered resolution for time intervals older than 14 ka BP because more recent intervals often have a significantly higher resolution. The selection criteria varied depending on the source type and time interval. For example, for records that only cover the Last Glacial Cycle, we select those with a maximum resolution of 200 years or better, while older records in our database have a resolution no worse than 400 years. However, exceptions were made for records from undersampled regions, such as the Guliya ice core[22] and several lake sediment records, and for exceptionally long and complete records, like the CENOGRID[23] and Chinese Loess Plateau[24] stacks.

While many of the paleosites listed in PaleoJump include multiple proxy types, we have focused on proxies that can be directly compared with climate models: oxygen isotopes reflecting changes in past temperatures, sea level, and precipitation; carbon isotopes containing information on past vegetation and the carbon cycle; aeolian deposits that include signatures of past precipitation, mineral aerosols, and atmospheric transport patterns; as well as other proxy-based estimates of past temperatures. We have mainly focused on the Last Glacial Cycle, due to the well-established evidence of past abrupt transitions—such as DO and Heinrich events—with most records also covering Holocene deglaciation. Other records extend further back in time, including DO-like events during earlier glacial cycles of the Quaternary, and earlier climatic events of the Cenozoic era, such as the Eocene–Oligocene Transition at 34 Ma or the PETM at 56 Ma. While PaleoJump provides global coverage with records from all continents and ocean basins, its spatial coverage is biased towards the North Atlantic region due to greater availability and to the strong impact of the DO events.

The well-known uncertainties in paleoclimate records need to be considered in building such a database. A key source of uncertainty is in their chronologies, as dating methods such as radiocarbon dating and layer counting have limitations and potential sources of error[25,26]. When independent dating is unavailable, "wiggle matching" is often performed to match records with other, well-dated records, but this method's use can be complicated by differences in local climate variability and time lags in climate signal propagation[27,28]. Additionally, recorded values of climate proxies may be affected by extra-climatic processes—physical, biological, and chemical—or by measurement errors. Interpretation of proxy records can also be challenging because a given

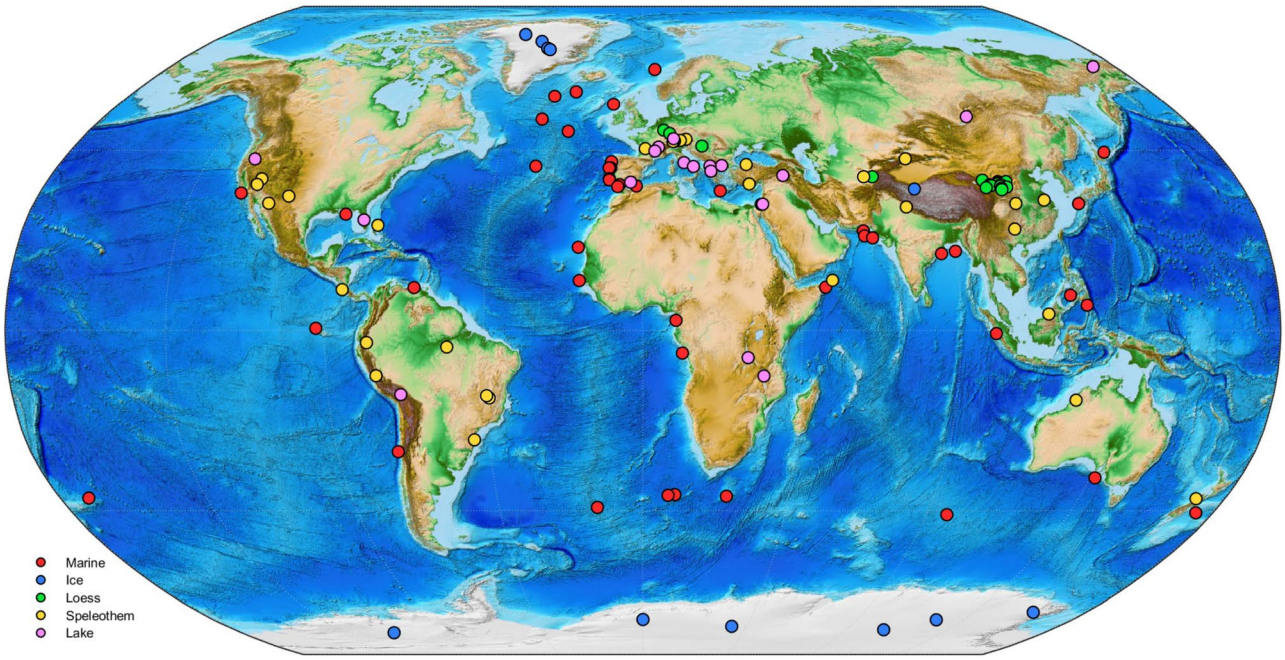

Figure 1. Map of the records included in the PaleoJump database and listed in the Supplementary Information. The five record sources—marine sediments, ice cores, terrestrial deposits, speleothems, and lake sediments—are identified in the legend by color. The land topography and ocean bathymetry are based on the ETOPO1 Global Relief Model data[175].

proxy variable may be influenced by multiple climatic processes[29–31], making it difficult to determine the specific climate conditions it represents.

In many of the records in PaleoJump, the chronology used for the original study has since been updated in more recent ones. When this is the case, we use the most recent age model's chronology. However, when the newer chronology does not cover the complete record, which is often the case, we use the older chronology. Furthermore, we did not attempt to harmonize and synchronize the age models among the records. These choices ensure that the most complete versions of the records are included in the database, while also allowing users to independently reproduce our analyses without having to reevaluate how harmonization was performed.

Five tables show the information for each record in the PaleoJump database and are included in the Supplementary Information[4,5,11,22–24,32–174] (Fig. 1).

Applying the KS test and RQA to TP identification

Given the diversity of the proxy records in the PaleoJump database, an objective, automated methodology is crucial for identifying and comparing TPs. Bagniewski et al.[19] formulated an augmented KS test, which they used to robustly detect and identify abrupt transitions during the last glacial cycle. These results were compared with results obtained using RQA, showing that the two methods are complementary, with KS test being more useful at detecting individual jumps and determining their exact dates, while RQA can help establish important transitions in a record's characteristic time scale. Here, we apply these two methods to a selection of records from the PaleoJump database and demonstrate the ability of the augmented KS test to accurately identify transitions in various types of paleoclimate records.

Kolmogorov–Smirnov (KS) test. The augmented KS methodology[19] is based on the nonparametric KS test[176]. A two-sample KS test is applied to two neighboring samples drawn from a proxy time series within a sliding window of length w. The commonality of the two samples is quantified by the the KS statistic D_{KS}[176,177]. A "jump" in the time series is identified at any point in time at which D_{KS} is greater than a cut-off threshold D_c. As the KS test can give very different results depending on the window length w being used, D_{KS} is calculated for different w's, varying between w_{min} and w_{max}. The values of the latter two parameters bracket the desired time scale at which a given paleorecord is to be investigated. Furthermore, smaller jumps in the time series may be the result of an error in the observed data or small-scale variability that occurs over time intervals shorter than the sampling resolution of the proxy record and they should be discarded. Thus, for a transition to be considered significant, the change in magnitude between the two samples (i, j) should exceed a threshold σ_c in their standard deviations (σ_i, σ_j). Finally, as the KS test requires a large enough sample size to be significant, its results are rejected if either of the two samples has a size n smaller than n_c.

At a time step at which all three conditions based on the parameters D_c, σ_c, and n_c are satisfied, an abrupt transition is identified. As the dates of such transitions often occur in clusters, the precise date for a transition within such a cluster is determined by the maximum D_{KS} value found within the corresponding time interval. When the maximum D_{KS} over a given interval is shared by several time steps, the one corresponding to the

maximum change in absolute magnitude is used; moreover, if there are several jumps of equal amplitude, then the one with the earliest date is used.

As the same transition may be found at slightly different dates depending on the window length that is used, we first identify the transitions detected with the longest window, which, given the larger sample size it accommodates, is the most statistically significant one. These transitions are then supplemented by those detected for the next-longest window and eventually for all other window lengths. For window w_i, we discard transitions identified at time t if the interval $\{t - w_i \leq t \leq t + w_i\}$ contains transitions that were previously identified with a greater window length. Finally, to identify transitions between dominant climate modes, such as the Stadial-Interstadial (GS–GI) boundaries, we use a running window to extract the upper and lower values from the time series and locate the transitions that mark a shift from one mode to the other.

The parameters D_c and σ_c are initially optimized following receiver operating characteristic analysis[178,179], and abrupt transitions so identified for the NGRIP ice core $\delta^{18}O$ record are further compared with the change points identified using visual inspection by Rasmussen et al.[131].

Recurrence Quantification Analysis (RQA). The KS test results are next compared with RQA results[20,21,180]. Here, the Recurrence Plot (RP) for a time series $\{x_k : k = 1, \ldots, K\}$ is given by a square pattern in which both axes represent time. A dot is entered into a position (i, j) of the matrix $\mathbf{R}$ when $|x_i - x_j| < \varepsilon$, with ε being the recurrence threshold. Thus, the RP appears as a square matrix $\mathbf{R}$ of dots. For details on how ε is determined, see Marwan et al.[21] and Bagniewski et al.[19].

Eckmann et al.[20] showed that purely visual RP typologies provide useful information about a time series. However, RQA allows for a more objective way of inferring recurrence[21,180], by quantifying selected recurrence characteristics. One of the simplest RQA criteria is the recurrence rate (RR), namely the density of dots within the recurrence plot: RR describes the probability of states of the system recurring within a particular time interval. By evaluating RQA measures such as RR in a sliding window, it is possible to identify changes in the time series. Low RR values correspond to an unstable behavior of the system, and hence abrupt transitions in a time series may be identified by local RR minima.

An important advantage of the recurrence method is that it does apply to dynamical systems that are not autonomous, i.e., that may be subject to time-dependent forcing[20]. The latter is certainly the case for the climate system in general[181–184] and, in particular, on the time scales of 10-100 kyr and longer, which are affected strongly by orbital forcing[185].

For a more comprehensive description of both the augmented KS test and RQA, see Bagniewski et al.[19].

Examples of usage

Here we show the results of the augmented KS test methodology[19], as applied to records of different timescales, resolutions, and periodicities. Plots of the detected transitions, along with files listing their dates are included in the PaleoJump database; the same is available for other records as well.

Methodology. We apply the augmented KS test to six records, given in Table 1, from each of the proxy types listed in Supplementary Tables 1–5. In addition to these six records, we include the results obtained for the NGRIP ice core, which have been published in Bagniewski et al.[19], and compare the latter with the three records of the last glacial cycle in the table, to wit MD03-2621, Paraiso Cave, and ODP893A.

The KS test parameters vary depending on a record's time resolution and on the length of its age interval. For the records covering the last glacial cycle (MD03-2621, Paraiso Cave, and ODP893A), we use the same parameter values as used for the NGRIP record in Bagniewski et al.[19], i.e., $D_c = 0.77, \sigma_c = 1.9, n_c = 3, w_{\min} = 0.1$ kyr, and $w_{\max} = 2.5$ kyr. For the records spanning longer time intervals with a lower temporal resolution, we use longer window lengths $w_{\min}$ and $w_{\max}$, thus shifting the focus of our analysis to longer time scales. For the U1308 benthic $\delta^{18}O$ and Lake Ohrid TIC records, we use a w-range of 2 kyr to 20 kyr. This allows us to focus on the glacial-cycle variability, as the record's resolution is too low to properly identify DO events, particularly for data older than 1.5 Ma BP, when the U1308 record's resolution is lower than for more recent data. For the CENOGRID record, we perform two separate analyses, one with a w-range of 1 Myr to 4 Myr to determine the Quaternary's major

Type	Site name	Location	Depth/elevation	Age	Res.	Proxy
Marine	ODP893A[87,88]	34.28, -120.03	576 m	65–0 ka	41 y	pla $\delta^{18}O$
Marine	MD03-2621[64]	10.678, -64.972	847 m	109–6 ka	0.1 y	reflectance
Marine	U1308[95]	49.878, -24.238	3871 m	3143–0 ka	118 y	ben $\delta^{18}O$
Marine	CENOGRID[23]	N/A	N/A	67.1–0 Ma	2000 y	ben $\delta^{18}O$
Terrestrial	Paraiso (PAR07)[165]	-4.067, -55.45	60 m	45–18 ka	21 y	$\delta^{18}O$
Terrestrial	Lake Ohrid[137]	41.049, 20.715	693 m	1.36–0 Ma	208 y	TIC
Ice	NGRIP[131]	75.1, -42.32	2925 m	122–0 ka	20 y	$\delta^{18}O$

Table 1. Records analyzed using the augmented KS test[19], ordered by geological type and temporal scale; the nature of the records is indicated in the last column by the abbreviations ben = benthic, pla = planktonic, and TIC = Total Inorganic Carbon.

climatic shifts, and one with a w-range of 0.02 Myr to 2.5 Myr, which covers the orbital time scale. Note that, in paleoclimate studies, one distinguishes between units of absolute time, such as kyr or Myr, and units of age, such as ka BP or Ma BP, where 'BP' stands for "before present."

Results for individual records. We chose the MD03-2621 reflectance record from the Cariaco Basin in the Caribbean for having a very high resolution and for its importance in studying the effect of DO events on the migrations of the intertropical convergence zone (ITCZ). The record is shown in Fig. 2 and it has been used previously to assess teleconnections between the North Atlantic basin and the Arabian Sea[64]. When the ITCZ migrates southward during stadials, northeasterly Trade winds lead to upwelling of cool, nutrient-rich waters in the Caribbean; as the ITCZ migrates northward during interstadials, heavy convective rainfall leads to increased runoff from South America's north coast, delivering detrital material to the Cariaco Basin[64,186]. As a result, the color reflectance in the core alternates between light-colored sediments, rich in foraminiferal carbonate and silica, and darker sediments abundant in detrital organic carbon. These changes in the marine sediments are proxies for the prevailing atmospheric circulation regime, and the meridional position of the ITCZ in the region, which are both linked to the glacial-interglacial variability.

For the KS analysis, a 20-year moving average of the MD03-2621 record is calculated in order to align its resolution with that of the NGRIP record. Our analysis does identify the "classical" DO events, as seen in the NGRIP record[19,131]. There is, however, no direct relationship in the identified longer-scale warm (grey bars) and cool intervals: For instance, some events appear to be merged in Fig. 2, e.g., GI-23 and 22, GI-16 and 15, GI-14 and 13, GI-10 and 9, and GI-4 and 3, while some events detected here, between 68 and 66 ka BP, are not identified in NGRIP, and GI-2 is much longer than in NGRIP.

The RQA analysis[21,180], shown in Fig. 3, does identify the major transitions in the MD03-2621 reflectance record, including the relative significance of each. It does not, however, resolve smaller transitions that occur at the centennial time scale. Please see Bagniewski et al.[19] for the explanation of the recurrence rate used to identify the transitions in the figure's panel (c).

The CENOGRID stack of benthic δ^{18}O[23] shown here in Fig. 4 is a highly resolved 67 Myr composite from 14 marine records. Westerhold et al.[23] distinguished four climate states—Hothouse, Warmhouse, Coolhouse, and Icehouse—in this record, largely following changes in the polar ice volume. The composite in the figure[23] reconstructs in detail Earth's climate during the Cenozoic era, at a higher time resolution than the earlier compilation of Zachos and colleagues[187].

Our KS analysis in Fig. 4a uses a window width $1 \leq w \leq 4$ Myr and it identifies four major transitions towards higher δ^{18}O values and two towards lower ones. The oldest transition, at 58 Ma BP, is characterized by a shift from the moderately warm climate prevailing at the beginning of the Cenozoic to the hot conditions marked by the Early Eocene Climate Optimum between 54 Ma and 49-48 Ma BP. The second transition corresponds to the short but intense warm event known as the PETM, the Cenozoic's hottest one. The third transition marks the end of this hot interval and the return to the milder and relatively stable conditions that prevailed between 67 Ma and 58 Ma BP.

The fourth transition, at 34 Ma, is the Eocene–Oligocene Transition, the sharp boundary between the warm and the hot climatic conditions in the earlier Cenozoic and the Coolhouse and then Icehouse conditions prevailing later on[188]. As this transition marks a major shift in the Earth's climate dynamics, it is a candidate for a major TP in Earth's climate history[189]. The fifth transition, at 14 Ma BP, ends a rather stable climate interval between 34 Ma and 14 Ma, characterized by the build up of the East Antarctic ice sheet[190,191]. This transition also marks the start of an increasing trend in benthic δ^{18}O values[192,193]. The final transition marks the start of the Icehouse world and it is characterized by the emergence and development of the Northern Hemisphere ice sheets.

Using a reduced window length on the last 26 Myr of the CENOGRID benthic record, many more abrupt transitions are detected in Fig. 4b. In particular, higher variability in the δ^{18}O signal and much more frequent transitions are found during two intervals, namely 71 transitions over the last 3.5 Myr and 77 transitions between 20 Ma BP and 13 Ma BP. In contrast, the intervals 67–20 Ma BP and 13–3.5 Ma BP are characterized by a lower frequency of detected transitions, with 112 and 13 transitions, respectively. The former one of the two intervals with many jumps includes the Quaternary Period, which started 2.6 Myr ago and is well known for its high climate variability, due to the presence of large ice masses in the system[6,194].

The interval 20–13 Ma BP, on the other hand, coincides with the exclusive use of the U1337 and U1338 records in constructing the CENOGRID stack, both of which are located in the eastern tropical Pacific. Higher sedimentation rates in these two cores might contribute to the higher variability δ^{18}O observed in the stack record over this interval. For transitions detected with the shorter window for the entire CENOGRID stack, please see Fig. S1 in the Supplementary Information.

The δ^{18}O record from the Paraiso Cave in the Amazon rainforest reveals a relationship between shifts in global temperature and changes in rainfall patterns in the region; see Fig. 5. The record shows that the Amazon basin experienced drier conditions during the last glacial period, most probably due to the lower temperatures. The record exhibits reduced precipitation during DO interstadials and increased precipitation during stadials, a pattern that negatively correlates with Chinese speleothem records[55], suggesting a phase opposition in rainfall between the two regions. The abrupt shifts in precipitation during DO events suggest that the Amazonian climate subsystem may exhibit bistability, making it a potential tipping element as changes in precipitation may lead to forest dieback[195].

Results for core intercomparisons. In Fig. 6, we compare four paleorecords of different types and from distinct locations: NGRIP δ^{18}O, MD03-2621 reflectance, Paraiso Cave δ^{18}O, and ODP893A planktic δ^{18}O from the Santa Barbara Basin. Overall, the abrupt transitions in the four records appear to be fairly synchronous, with

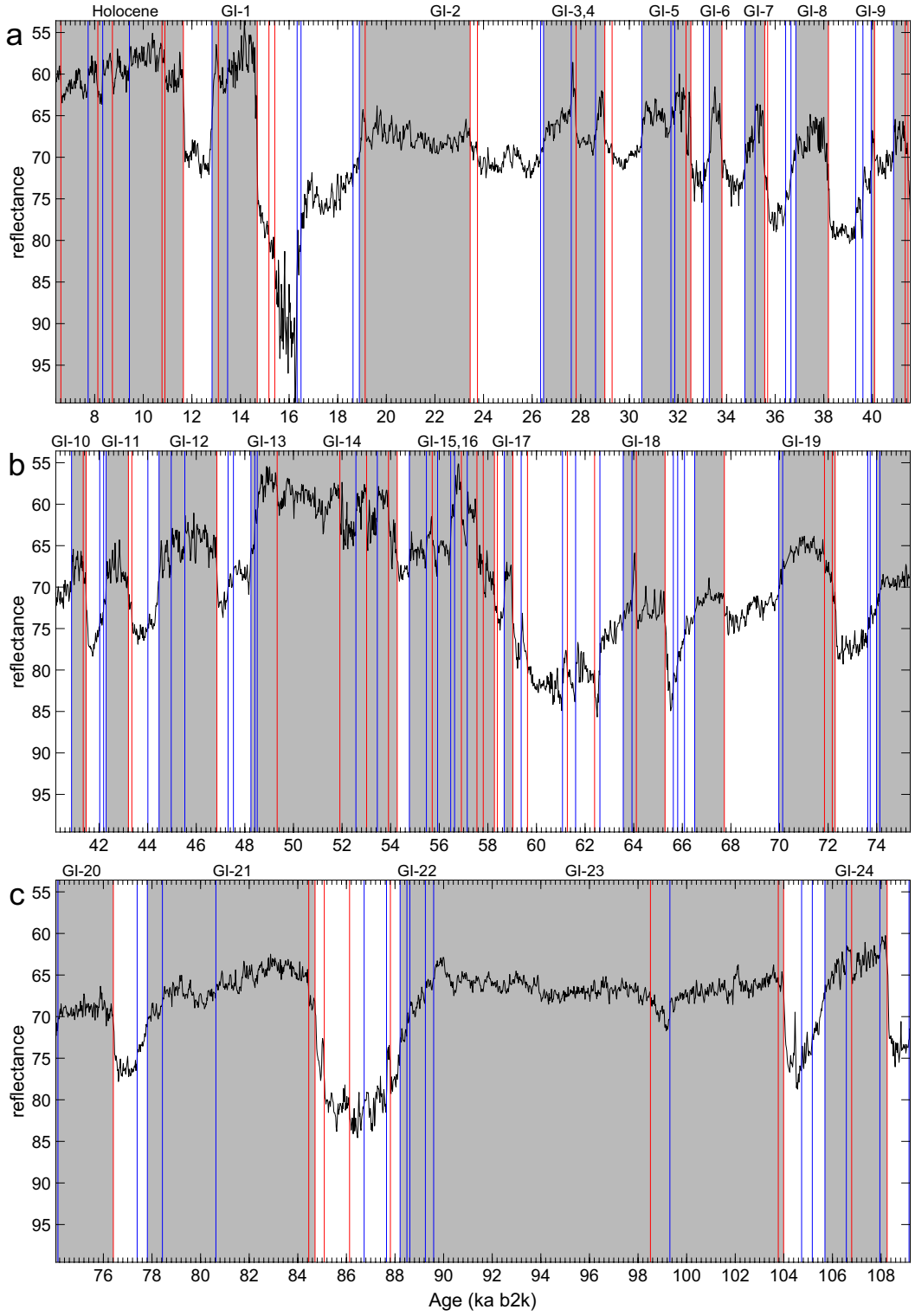

Figure 2. MD03-2621 marine sediment core: (**a**) 6.4–41.6 ka b2k; (**b**) 40.2–75.4 ka b2k; and (**c**) 74–109.2 ka b2k. The black solid line is the core reflectance[64], with the vertical axis reversed. Vertical lines represent transitions detected by the KS test of Bagniewski et al.[19], with colors indicating the direction of the jumps. In this figure, red lines represent a warming event, while blue lines represent a cooling event. In other figures, the meaning of the colors may vary. Grey bars denote warm episodes. Note that all time axes in this paper follow the geological custom of pointing into the past.

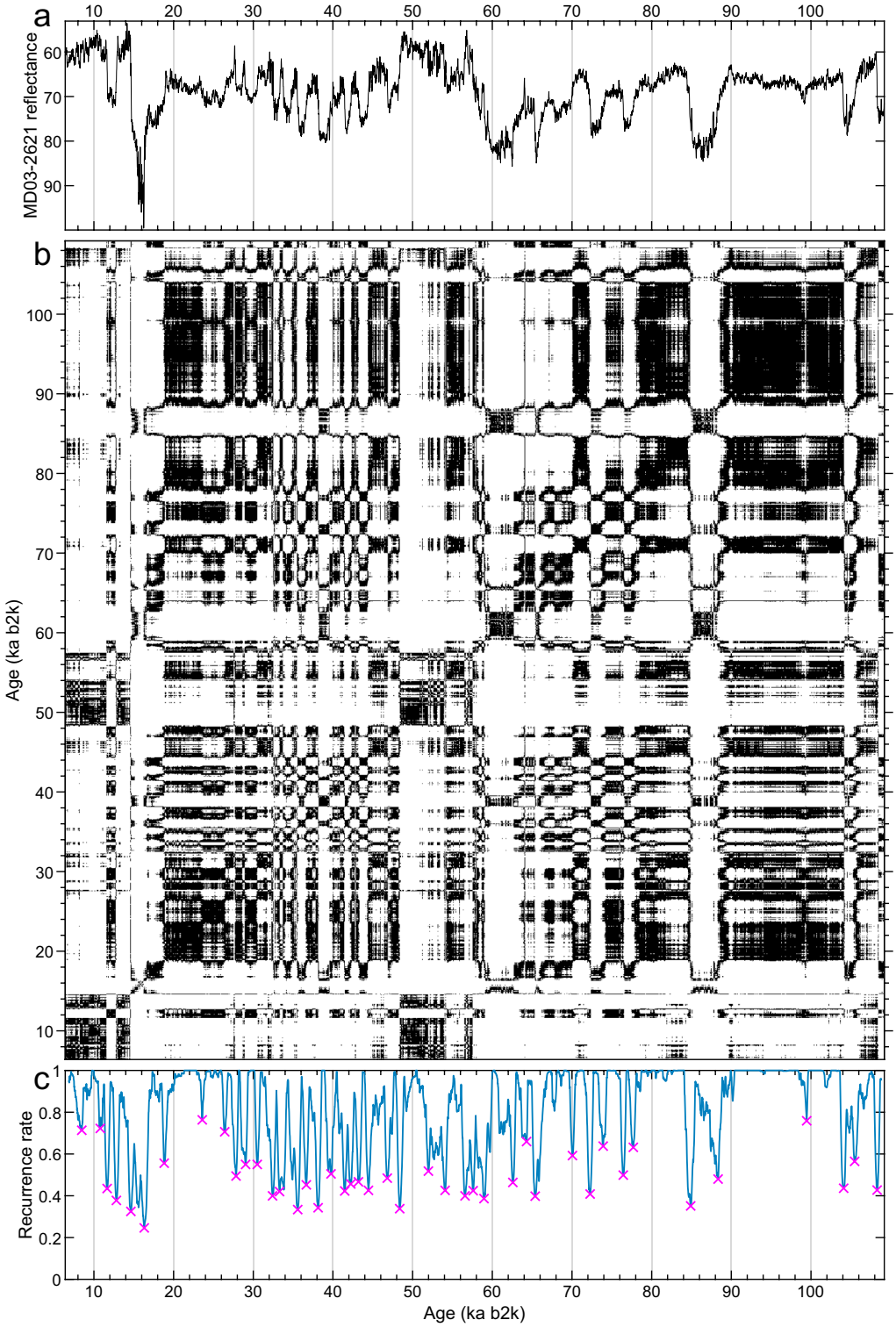

Figure 3. Recurrence Quantification Analysis (RQA)[21,180] for the MD03-2621 reflectance record[64]. (**a**) Time series with vertical axis as in Fig. 2; (**b**) recurrence plot (RP); and (**c**) recurrence rate. Magenta crosses in (**c**) represent the transitions identified by the RQA.

the main Greenland DO events from NGRIP also observed for the two marine records and the one speleothem record. The transitions that correspond to Greenland interstadials (GIs) GI-12 to GI-3[131] are identified in all four records, with only a few exceptions: GI-3 is not identified for the ODP893A record, due to an insufficient

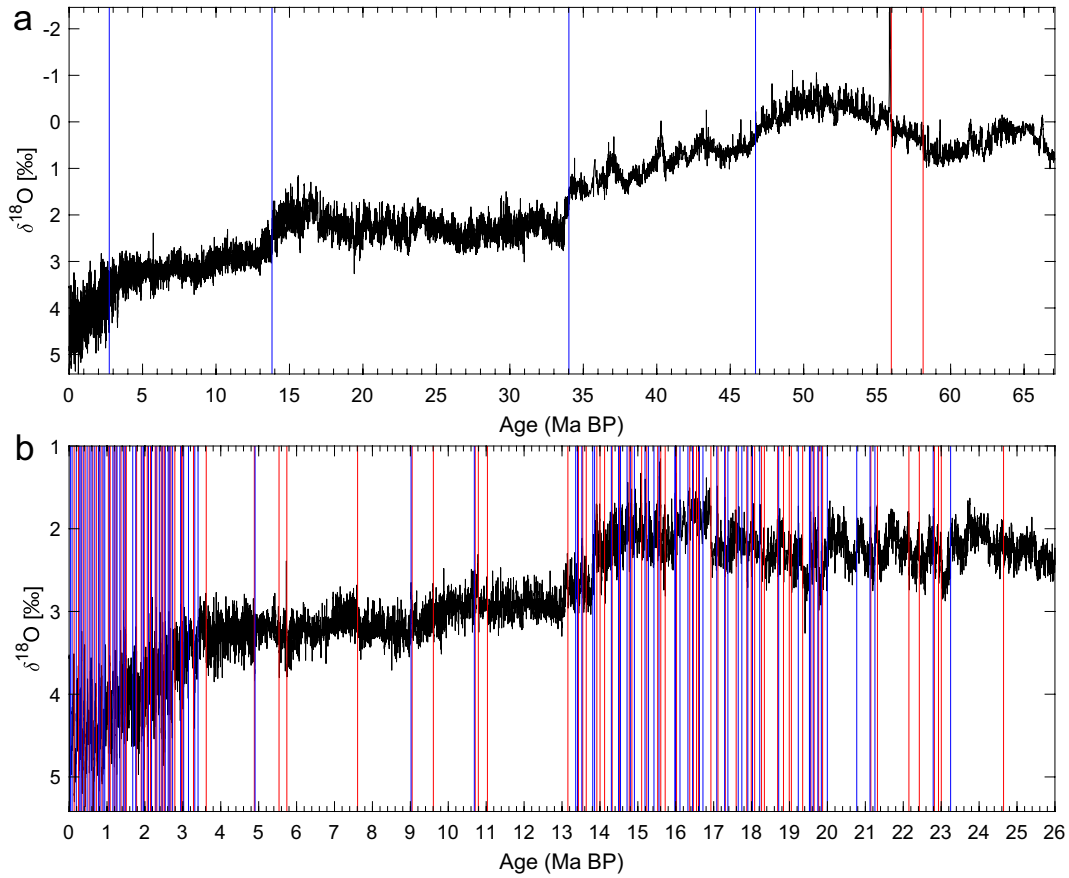

Figure 4. CENOGRID stack of benthic $\delta^{18}O$[23]. Vertical lines represent transitions detected by the KS test[19], with colors indicating the direction of the jumps. Grey bars represent warm episodes. (**a**) Transitions detected for the entire record using a window *w* range of 1–4 Myr, and (**b**) transitions detected for the interval 26–0 Ma BP using a *w* range of 0.02–2.5 Myr; see also the earlier subsection on "Methodology." The vertical axes are reversed.

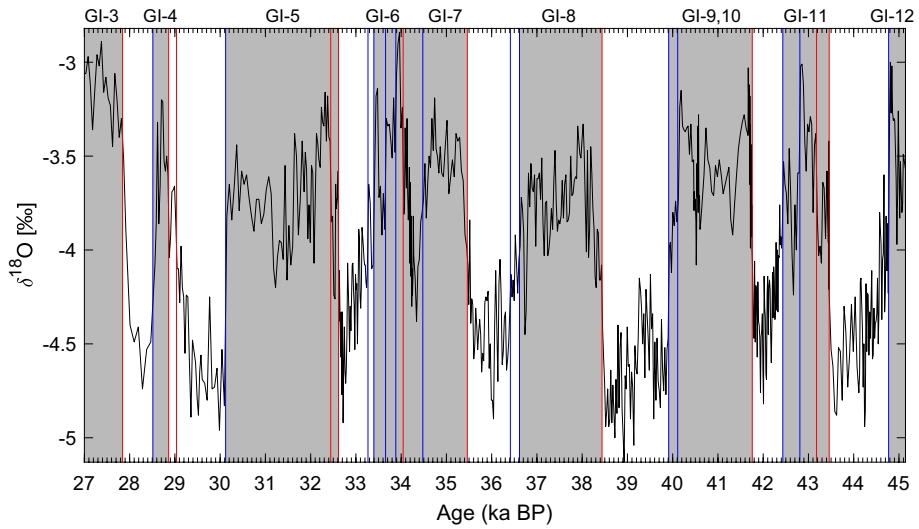

Figure 5. Paraiso Cave (PAR07) $\delta^{18}O$[165]. Vertical lines represent transitions detected by the KS algorithm[19], with colors indicating the direction of the jumps. Grey bars represent dry interglacial conditions.

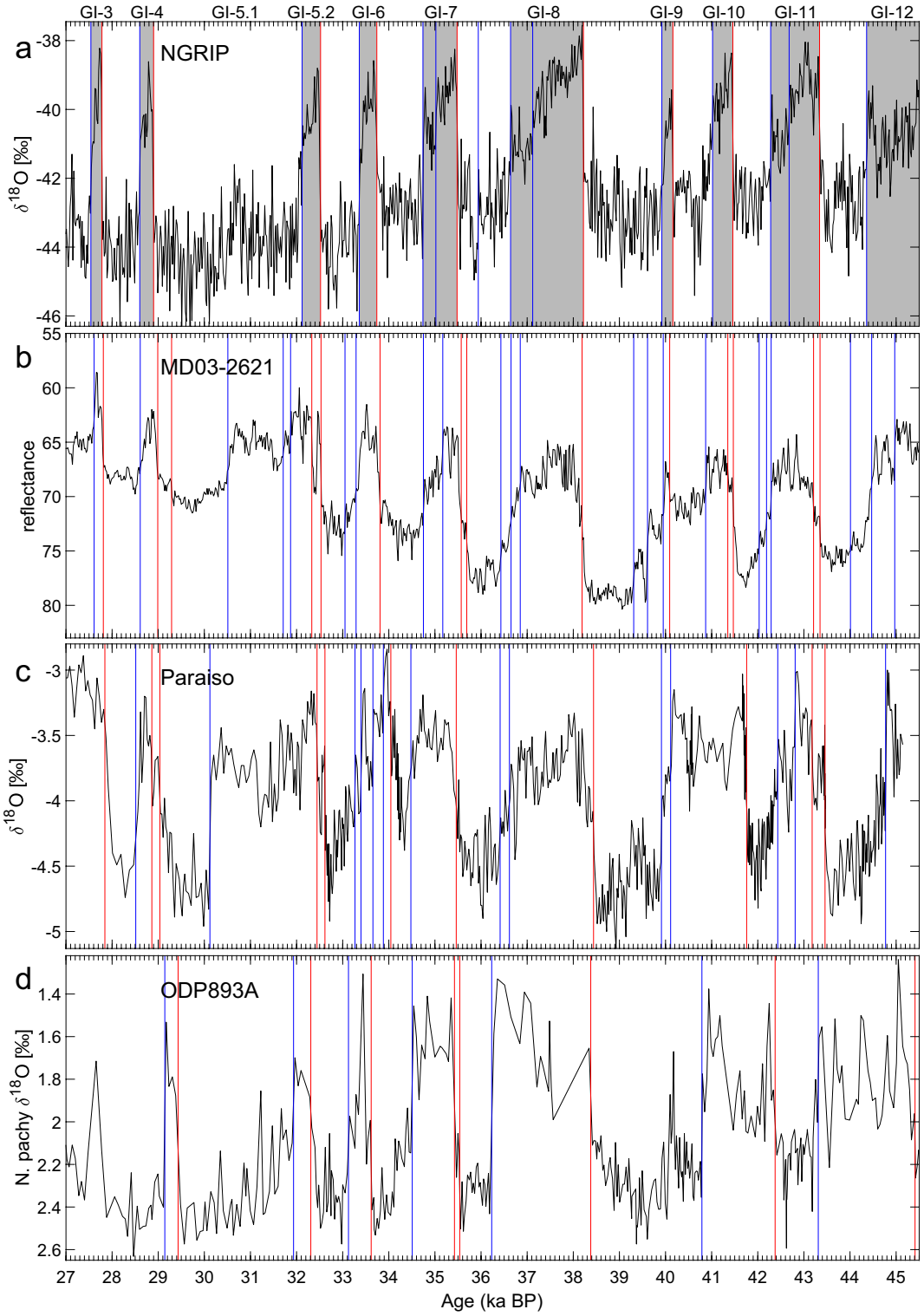

Figure 6. Comparison of four paleorecords over the 45.5–27 ka BP interval: (**a**) NGRIP ice core $\delta^{18}O$[131]; (**b**) MD03-2621 marine sediment reflectance[64]; (**c**) Paraiso Cave (PAR07) $\delta^{18}O$[165]; and (**d**) ODP893A marine sediment *N. pachyderma* $\delta^{18}O$[87,88]. Vertical lines represent detected transitions, with colors indicating the direction of the jumps. Grey bars in panel (**a**) represent interstadials identified for the NGRIP $\delta^{18}O$ record by Bagniewski et al.[19]. Note that the "ka BP" time unit, where the 'Present' is defined as the year 1950, applies only to the Paraiso and ODP893A records. The NGRIP and MD03-2621 records use the "ka b2k" time scale, where 'b2k' refers to the year 2000 as the origin of past times. The vertical axes in (**b, d**) are reversed.

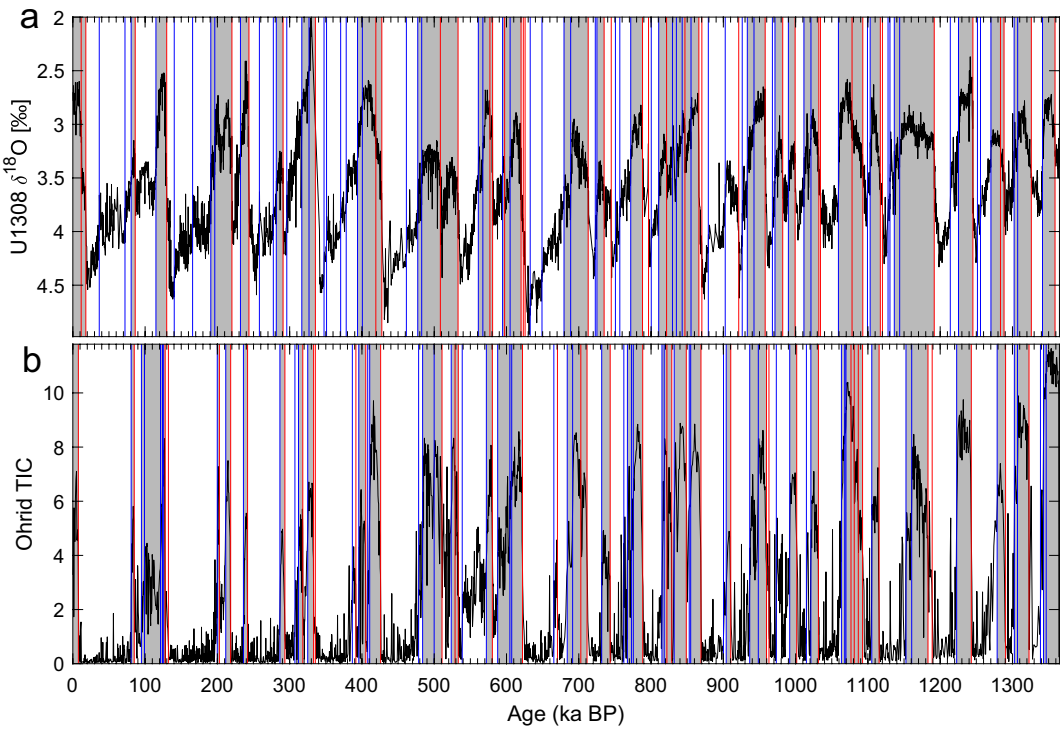

Figure 7. Comparison of the benthic *Cibicidoides sp.* δ^{18}O record in (**a**) the U1308 marine-sediment core[95] and (**b**) Lake Ohrid TIC[137]. Vertical lines represent transitions detected by our KS methodology[19], with colors indicating the direction of the jumps. Grey bars correspond to interglacials (odd-numbered MISs) and white bars correspond to glacials (even-numbered MISs). The vertical axis in (**a**) is reversed.

number of data points; and GI-5.1 is not identified in any record, except as a cooling event in MD03-2621 and in Paraiso cave. Also, GI-10 and GI-9 appear as a single interstadial in the Paraiso cave and ODP893A records, which is probably due to a decreased time resolution observed in both records during this time interval.

Finally, Fig. 7 shows the comparison between the U1308 benthic δ^{18}O record and the Lake Ohrid Total Inorganic Carbon (TIC) record over a 1.4 Myr time interval that includes multiple glacial-interglacial transitions.

The U1308 benthic δ^{18}O record in panel (a) of the figure is a 3.1 Myr record located within the ice-rafted detritus belt of the North Atlantic[196]. This record is a proxy for deep-water temperature and global ice volume, and it has enabled a detailed reconstruction of the history of orbital and millennial-scale climate variability during the Quaternary; it documents the changes in Northern Hemisphere ice sheets that follow the glacial–interglacial cycles, as well as mode transitions identified at 2.55 Ma, 1.5 Ma, 1.25 Ma, 0.65 Ma and 0.35 Ma BP[95,197]. Here, we only show the 1.4–0 Ma BP time interval that corresponds to the length of the Lake Ohrid record. For the full 3.1 Myr U1308 record, please see Fig. S2 in the Supplementary Information.

The 1.25–0.65 Ma BP interval in the figure corresponds to the Mid-Pleistocene Transition, characterized by an increase in the amplitude of the glacial–interglacial fluctuations and a shift from a predominantly 40 kyr to a predominantly 100 kyr periodicity; see Reichers et al.[185] and references therein. The abrupt transition at 0.35 Ma marks the start of the strongest interglacial of the record, which corresponds to the marine isotope stage (MIS) 9. Here, our KS analysis agrees with the well established marine isotope stratigraphy of Lisiecki and Raymo[198] by detecting rapid warmings that correspond to the classical terminations leading to interglacials, as well as rapid coolings that initiate glacial stages.

The Lake Ohrid TIC record in Fig. 7b shows glacial–interglacial variability in biomass over the past 1.4 Myr. Here, our KS analysis shows numerous abrupt transitions towards high TIC intervals that correspond to interglacial episodes, as well as matching ones of opposite sign. The interglacials are associated with forested environmental conditions that are consistent with odd-numbered MISs, as was the case for the U1308 record in the figure's panel (a). The glacial episodes, to the contrary, correspond to forestless conditions, that, according to the available timescale, are consistent with even-numbered MISs.

Discussion

The two methods. The augmented KS test of Bagniewski et al.[19] has detected abrupt transitions on different time scales in a variety of paleorecords. These include the NGRIP ice core, the Paraiso Cave speleothem, and the MD03-2621 and ODP893A marine sediment cores for the last glacial cycle; the U1308 marine sediment core and Lake Ohrid TIC for the Middle and Late Pleistocene; and the CENOGRID marine sediment stack for the Cenozoic Era. While possible mechanisms giving rise to the observed variability in these records have been dis-

cussed in previous studies, the objective, precise and robust dating of the main transitions using the augmented KS test may allow a more detailed and definitive analysis and modeling.

The transitions identified for the MD03-2621 reflectance record with the RQA methodology[20,21,180] do correspond to a subset of those found with the KS test, but several smaller-scale transitions identified by the latter have not been found with the former method. As discussed in Bagniewski et al.[19], recognizing the transition points by RQA becomes increasingly difficult at time scales shorter than the window length. The RQA approach, though, does allow one to quantify the magnitude of each transition, and it may thus be useful for identifying key transitions. Moreover, RPs may be helpful in illustrating changes in periodicity.

Interpretation of findings. The high-resolution MD03-2621 reflectance record from the Cariaco Basin[64] in Fig. 2 shows abrupt transitions that are largely in agreement with those detected by our KS test for the NGRIP record. Desplazes et al.[64] have argued that these transitions are driven by the ITCZ displacements that occurred primarily in response to Northern Hemisphere temperature variations. These authors indicated that the ITCZ migrated seasonally during mild stadials, but was permanently displaced south of the Cariaco Basin during the colder stadial conditions. The very high resolution of the MD03-2621 record allows a detailed comparison with the transitions identified for the NGRIP record. The fact that several small-scale NGRIP transitions are not identified by our KS test in the MD03-2621 record suggests that a TP linked to ITCZ migration was not crossed during these events. Furthermore, the KS test does reveal transitions that have not been recognized previously in either record[131], e.g., at 86.15 ka BP, which we find in both the NGRIP and MD03-2621 records.

In the 67-Myr CENOGRID stack (Fig. 4) of benthic $\delta^{18}O$[23,187], we identified four major cooling transitions that culminate with the start of the Pleistocene, as well as two warming transitions, including the PETM. These major jumps agree with those identified in Westerhold et al.[23]. However, using a shorter window length, many more transitions were detected during the Pleistocene, well known for its higher climate variability[6,194], as well as during the early Miocene, i.e., between the Oligocene-Miocene transition at 23 Ma BP[199–201] and the mid-Miocene transition at 14 Ma BP[191]. A possible reason is the fact that the 20–13 Ma BP interval in the stack has been constructed using records from the eastern Tropical Pacific. This region has been characterized by high upwelling rates and sedimentation rates in the past[202]. While the CENOGRID composite has a uniform resolution, higher sedimentation rates could affect the resolution of the original records and, therewith, even the variability seen in lower-resolution sampling.

It follows from these remarks on Fig. 4a, b that variations in resolution of the data, which can arise from various factors including measurement techniques and source region characteristics, can have a considerable effect on the frequency of detected transitions. These factors can significantly impact the reliability of transition detection methods, thus highlighting the need for caution when using individual records as proxies for global climate. While statistical indicators allow us to quantify jumps in the data without any climatic context being provided, it is important to consider the limitations of such an approach, and to supplement it with an independent understanding of the proxy data whenever possible. By doing so, we can better contextualize and understand the implications of these jumps.

The Paraiso Cave record[165] from the eastern Amazon lowlands in Fig. 5 shows drier conditions during interglacials, with abrupt transitions matching those that correspond to the DO events identified in the NGRIP ice core record. The Amazon record is also in fairly good agreement with the nearby MD03-2621 marine sediment record. Notably, several of NGRIP's DO events appear combined in both records, namely GI-5.2 and GI-5.1, as well as GI-10 and GI-9, which might indicate that a climate change event over Greenland did not trigger a tipping event in the Amazon basin. Alternatively, the first merging may question the separation of the classical GI-5 event[203] into two distinct events, 5.2 and 5.1.

The comparison of four records on the same time scale in Fig. 6 demonstrates that a signal of abrupt climate change is detected when using the KS method with similar accuracy for different types of paleodata. The differences in the dates of the transitions may be largely explained by the use of different age models in each of the records, with MD03-2621 fine-tuned to the NGRIP chronology, and ODP893A fine-tuned to the GISP2 chronology, while the NGRIP and Paraiso Cave records were independently dated. Notably, ODP893A data prior to GI-8 appear misaligned with the other three records. The chronology of jumps in ODP893A indicates that the warm interval between 42.4 ka BP and 40.8 ka BP may correspond to an event spanning GI-10 and GI-9, while the warm interval between 45.3 ka BP and 43.3 ka BP may correspond to GI-11.

It is important to keep in mind that age estimates of many paleoclimate records, including some of those discussed here, are often not determined through independent methods, but rather are "tuned" or wiggle-matched to other records, such as the global benthic $\delta^{18}O$ stack[198] or the NGRIP $\delta^{18}O$ record[131]. As the abrupt jumps in these records are themselves used as tie-points, it is expected that the KS test would show a similarity in the timing of jumps in records that were tuned to the same reference record. Therefore, any differences in the timing of transitions between these records should not be taken as indicative of the chronology of events, but rather as a result of differences between the KS method and the transition detection method used in the wiggle matching process. This fact should be taken into consideration when comparing records that have not been independently dated.

In addition to the classical GI transitions, several additional jumps are identified in each of the marine and cave records. These jumps may be the representative of local climate changes or, in some cases, be artifacts of sampling resolution or measurement error. Stronger evidence for a local or regional event may be obtained when comparing two nearby records, like the Paraiso Cave in the Amazon and the MD03-2621 marine record from the Cariaco Basin. In both records, the start of GI-5.2 is represented as two warming transitions, in contrast with the NGRIP and ODP893A records, where only one sharp transition is present. Likewise, the end of GI-9 in the two tropical, South American records appears as two successive cooling events. These results point to the potential

of using the KS method to improve fine-tuning the synchroneity of two or more records, when an independent dating method is not available.

The comparison in Fig. 7 of KS-detected transitions in marine core U1308[95] and in Lake Ohrid TIC[137] identifies the transitions between individual glacials and interglacials. In the two records, the transitions are well identified, despite the resolution of the two being different, and they offer a precise dating for the chronology of the past glacial cycles. The transitions are overall in good agreement between the two records. Still, the warm events in Lake Ohrid are essentially atmospheric and thus have often a shorter duration than in the marine record, while cooling transitions precede those in the deep ocean by several thousand years. This could indicate that a significant time lag is present, either in ice sheet growth in response to atmospheric cooling, or in the propagation of the cooling signal into the deep North Atlantic.

Furthermore, there are atmospheric interglacial episodes missing in the oceanic U1308 record. This mismatch between the lake record[137] and the marine one[95] could be attributed to the fact that the KS test does sometimes find more transitions in one record than in another one, even for the same type of proxy and within the same region. Such occurrences may be due to the local environment, the sampling method, or some aspect of the KS method itself. When this is the case, it is important—although not always feasible—to obtain additional records covering a similar time interval with a similar resolution, in order to shed further light on the mismatch between the two original records. It should be noted that this study analyzed only one proxy type from each location. A more comprehensive representation of past transitions could be achieved by investigating different proxy records from the same core. For example, in contrast to the Rasmussen et al.[131] study of the NGRIP record, which analyzed both the $\delta^{18}O$ and Ca^{2+} proxies, this study only utilized $\delta^{18}O$ (Fig. 6a), which is a likely reason for not detecting the GI-5.1 event.

Concluding remarks

The carefully selected, high-quality paleoproxy records in the open-source PaleoJump database[18], https://paleojump.github.io, have different temporal scales and a global spatial coverage; see again Fig. 1. These records provide an easily accessible resource for research on potential tipping elements in Earth's climate. Still, major gaps in the marine sediment records exist in the Southern Hemisphere, especially in the Indian and Pacific Oceans. Only sparse terrestrial data are available from the high latitudes in both hemispheres, due to the recent glaciation. The only data from the African continent come from two East African lake sediment records. Even though much information is at hand from the more than 100 sites listed in this paper, more records are needed to fill geographical and temporal gaps, especially in the Southern Hemisphere.

The examples given in the paper on abrupt-transition identification demonstrate the usefulness of the records included in PaleoJump for learning about potential tipping events in Earth's history and for comparing such events across different locations around the world. The accessibility of such high-quality records is an invaluable resource for the climate modeling community that requires comparing their results across a hierarchy of models[184,204] with observations.

We also demonstrated the usefulness of the KS test[19] for reconstructing the chronology of Earth's main climatic events. The newly developed tool for automatic detection of abrupt transitions may be applied to different types of paleorecords, allowing to objectively and robustly characterize the tipping phenomenon for climate subsystems already suspected of being subject to tipping[9], but also to identify previously unrecognized tipping elements in past climates. The observational descriptions of tipping that can be obtained from PaleoJump using our KS methodology, combined with the application of Earth System Models, can help improve the understanding of the bifurcation mechanisms of global and regional climate and identify possible TPs for future climates.

Our results also indicate that paleorecord interpretations may vary, since the abrupt transitions identified in them will depend on the time scale and type of variability that is investigated. For example, the KS method's parameters[19] may be changed when studying different proxy record resolutions, affecting the frequency and exact timing of the TPs that are identified.

The agreement in timing and pattern between jumps in distinct records can confirm the correctness of each record separately, as well as of the inferences on climate variability drawn from these jumps. Specifically, the ability of the KS method to identify matching small-scale transitions in different high-resolution records may be used to validate these transitions as being the result of genuine global or regional climatic events, as opposed to just sampling errors. Furthermore, significant differences in records that are, overall, in good agreement with each other may help decode the chronology of tipping events or an approximate range for a tipping threshold. A fortiori, the differences in timing and pattern between jumps in distinct records that we also found emphasize the importance of a consistent dating methodology.

In a potential second step, the transition detection tools presented here could be used for harmonizing and synchronizing the records of the PaleoJump database, in a way that resembles the work conducted by several research teams in recent years[13,159,205–208]. Doing so would facilitate interpretating the abrupt changes in these records.

The broad spatial coverage of the PaleoJump database[18], https://paleojump.github.io, with its records that vary in their nature—ice, marine and land—as well as in their length and resolution, will facilitate research on tipping elements in Earth's climate, including the polar ice sheets, the Atlantic Meridional Overturning Circulation, and the tropical rainforests and monsoon systems. Furthermore, it will support establishing improved criteria on where and how to collect data for reliable early warning signals of impending TPs.

Data availability

The datasets analyzed during the current study are available through Zenodo (https://doi.org/10.5281/zenodo.6534031)[18] and on the PaleoJump website, (https://paleojump.github.io). The source code of the PaleoJump

website can be found on GitHub at (https://github.com/paleojump/paleojump). The codes used for KS and RQA analyses are part of the TiPES statistical toolbox, available on GitHub at (https://github.com/paleojump/TiPES_statistical_toolbox). The ETOPO1 Global Relief Model data[175] used for making Fig. 1 is available from NOAA at (https://www.ncei.noaa.gov/products/etopo-global-relief-model).

Received: 8 June 2022; Accepted: 27 February 2023
Published online: 18 March 2023

References

1. Dansgaard, W. *et al.* A new Greenland deep ice core. *Science* **218**, 1273–1277 (1982).
2. Johnsen, S. *et al.* Irregular glacial interstadials recorded in a new Greenland ice core. *Nature* **359**, 311–313 (1992).
3. Grootes, P. M., Stuiver, M., White, J., Johnsen, S. & Jouzel, J. Comparison of oxygen isotope records from the GISP2 and GRIP Greenland ice cores. *Nature* **366**, 552–554 (1993).
4. Shackleton, N. J., Hall, M. A. & Vincent, E. Phase relationships between millennial-scale events 64000–24000 years ago. *Paleoceanography* **15**, 565–569 (2000).
5. Genty, D. *et al.* Precise dating of Dansgaard–Oeschger climate oscillations in western Europe from stalagmite data. *Nature* **421**, 833–837 (2003).
6. Ghil, M. & Childress, S. *Topics in Geophysical Fluid Dynamics: Atmospheric Dynamics, Dynamo Theory, and Climate Dynamics* (Springer, Berlin, 1987). Reissued as an eBook in 2012.
7. Ghil, M. & Lucarini, V. The physics of climate variability and climate change. *Rev. Mod. Phys.* **92**, 035002 (2020).
8. Pearce, F. *With Speed and Violence: Why Scientists Fear Tipping Points in Climate Change* (Beacon Press, New York, 2007).
9. Lenton, T. M. *et al.* Tipping elements in the Earth's climate system. *Proc. Natl. Acad. Sci.* **105**, 1786–1793 (2008).
10. Scheffer, M. *et al.* Early-warning signals for critical transitions. *Nature* **461**, 53–59 (2009).
11. Sánchez Goñi, M. F. *et al.* The ACER pollen and charcoal database: a global resource to document vegetation and fire response to abrupt climate changes during the last glacial period. *Earth Syst. Sci. Data* **9**, 679–695 (2017).
12. Atsawawaranunt, K. *et al.* The SISAL database: A global resource to document oxygen and carbon isotope records from speleothems. *Earth Syst. Sci. Data* **10**, 1687–1713 (2018).
13. Jonkers, L. *et al.* Integrating palaeoclimate time series with rich metadata for uncertainty modelling: Strategy and documentation of the PalMod 130k marine palaeoclimate data synthesis. *Earth Syst. Sci. Data* **12**, 1053–1081 (2020).
14. Mulitza, S. *et al.* World atlas of late quaternary foraminiferal oxygen and carbon isotope ratios. *Earth Syst. Sci. Data* **14**, 2553–2611 (2022).
15. Judd, E. J. *et al.* The PhanSST global database of Phanerozoic sea surface temperature proxy data. *Sci. Data* **9**, 1–38 (2022).
16. Ghil, M. Hilbert problems for the geosciences in the 21st century. *Nonlinear Process. Geophys.* **8**, 211–211 (2001).
17. Wunderling, N., Donges, J. F., Kurths, J. & Winkelmann, R. Interacting tipping elements increase risk of climate domino effects under global warming. *Earth Syst. Dyn.* **12**, 601–619 (2021).
18. Bagniewski, W., Rousseau, D.-D. & Ghil, M. Paleojump (2022). https://doi.org/10.5281/zenodo.6534031.
19. Bagniewski, W., Ghil, M. & Rousseau, D.-D. Automatic detection of abrupt transitions in paleoclimate records. *Chaos* **31**, 113129 (2021).
20. Eckmann, J.-P., Kamphorst, S. O. & Ruelle, D. Recurrence plots of dynamical systems. *Europhys. Lett.* **4**, 973–977 (1987).
21. Marwan, N., Romano, M. C., Thiel, M. & Kurths, J. Recurrence plots for the analysis of complex systems. *Phys. Rep.* **438**, 237–329 (2007).
22. Thompson, L. G. *et al.* Tropical climate instability: The last glacial cycle from a Qinghai-Tibetan ice core. *Science* **276**, 1821–1825 (1997).
23. Westerhold, T. *et al.* An astronomically dated record of Earth's climate and its predictability over the last 66 million years. *Science* **369**, 1383–1387 (2020).
24. Sun, Y., Clemens, S. C., An, Z. & Yu, Z. Astronomical timescale and palaeoclimatic implication of stacked 3.6-myr monsoon records from the Chinese loess plateau. *Quat. Sci. Rev.* **25**, 33–48 (2006).
25. Boers, N., Goswami, B. & Ghil, M. A complete representation of uncertainties in layer-counted paleoclimatic archives. *Clim. Past* **13**, 1169–1180 (2017).
26. Goswami, B. *et al.* Abrupt transitions in time series with uncertainties. *Nat. Commun.* **9**, 1–10 (2018).
27. Blunier, T. & Brook, E. J. Timing of millennial-scale climate change in Antarctica and Greenland during the last glacial period. *Science* **291**, 109–112 (2001).
28. Skinner, L. & Shackleton, N. An Atlantic lead over Pacific deep-water change across Termination I: Implications for the application of the marine isotope stage stratigraphy. *Quat. Sci. Rev.* **24**, 571–580 (2005).
29. Shackleton, N. Oxygen isotope analyses and Pleistocene temperatures re-assessed. *Nature* **215**, 15–17 (1967).
30. McDermott, F. Palaeo-climate reconstruction from stable isotope variations in speleothems: a review. *Quat. Sci. Rev.* **23**, 901–918 (2004).
31. Bagniewski, W., Meissner, K. J., Menviel, L. & Brennan, C. E. Quantification of factors impacting seawater and calcite $\delta^{18}O$ during Heinrich Stadials 1 and 4. *Paleoceanography* **30**, 895–911 (2015).
32. Allen, J. R. *et al.* Rapid environmental changes in southern Europe during the last glacial period. *Nature* **400**, 740–743 (1999).
33. Allen, J. R., Watts, W. A. & Huntley, B. Weichselian palynostratigraphy, palaeovegetation and palaeoenvironment; the record from Lago Grande di Monticchio, southern Italy. *Quat. Int.* **73**, 91–110 (2000).
34. Ampel, L., Wohlfarth, B., Risberg, J. & Veres, D. Paleolimnological response to millennial and centennial scale climate variability during MIS 3 and 2 as suggested by the diatom record in Les Echets, France. *Quat. Sci. Rev.* **27**, 1493–1504 (2008).
35. Arienzo, M. M. *et al.* Bahamian speleothem reveals temperature decrease associated with Heinrich stadials. *Earth Planet. Sci. Lett.* **430**, 377–386 (2015).
36. Asmerom, Y., Polyak, V. J. & Burns, S. J. Variable winter moisture in the southwestern United States linked to rapid glacial climate shifts. *Nat. Geosci.* **3**, 114–117 (2010).
37. Bahr, A. *et al.* Oceanic heat pulses fueling moisture transport towards continental Europe across the mid-Pleistocene transition. *Quat. Sci. Rev.* **179**, 48–58 (2018).
38. Bar-Matthews, M., Ayalon, A., Gilmour, M., Matthews, A. & Hawkesworth, C. J. Sea-land oxygen isotopic relationships from planktonic foraminifera and speleothems in the Eastern Mediterranean region and their implication for paleorainfall during interglacial intervals. *Geochim. Cosmochim. Acta* **67**, 3181–3199 (2003).
39. Barbante, C. *et al.* One-to-one coupling of glacial climate variability in Greenland and Antarctica. *Nature* **444**, 195–198 (2006).
40. Barker, S. *et al.* 800,000 years of abrupt climate variability. *Science* **334**, 347–351 (2011).
41. Barker, S. & Diz, P. Timing of the descent into the last Ice Age determined by the bipolar seesaw. *Paleoceanography* **29**, 489–507 (2014).
42. Barker, S. *et al.* Early interglacial legacy of deglacial climate instability. *Paleoceanogr. Paleoclimatol.* **34**, 1455–1475 (2019).

43. Baumgartner, M. *et al.* NGRIP CH 4 concentration from 120 to 10 kyr before present and its relation to a $\delta^{15}N$ temperature reconstruction from the same ice core. *Clim. Past* **10**, 903–920 (2014).
44. Bazin, L. *et al.* An optimized multi-proxy, multi-site Antarctic ice and gas orbital chronology (AICC2012): 120–800 ka. *Clim. Past* **9**, 1715–1731 (2013).
45. Benson, L., Lund, S., Negrini, R., Linsley, B. & Zic, M. Response of north American Great basin lakes to Dansgaard–Oeschger oscillations. *Quat. Sci. Rev.* **22**, 2239–2251 (2003).
46. Beuscher, S. *et al.* End-member modelling as a tool for climate reconstruction-an Eastern Mediterranean case study. *PLoS ONE* **12**, e0185136 (2017).
47. Boch, R. *et al.* NALPS: A precisely dated European climate record 120–60 ka. *Clim. Past* **7**, 1247–1259 (2011).
48. Bolton, C. T. *et al.* North Atlantic midlatitude surface-circulation changes through the Plio-Pleistocene intensification of Northern Hemisphere glaciation. *Paleoceanogr. Paleoclimatol.* **33**, 1186–1205 (2018).
49. Burns, S. J., Fleitmann, D., Matter, A., Kramers, J. & Al-Subbary, A. A. Indian Ocean climate and an absolute chronology over Dansgaard/Oeschger events 9 to 13. *Science* **301**, 1365–1367 (2003).
50. Camuera, J. *et al.* Orbital-scale environmental and climatic changes recorded in a new 200,000-year-long multiproxy sedimentary record from Padul, southern Iberian Peninsula. *Quat. Sci. Rev.* **198**, 91–114 (2018).
51. Camuera, J. *et al.* Chronological control and centennial-scale climatic subdivisions of the Last Glacial Termination in the western Mediterranean region. *Quat. Sci. Rev.* **255**, 106814 (2021).
52. Camuera, J. *et al.* Past 200 kyr hydroclimate variability in the western mediterranean and its connection to the african humid periods. *Sci. Rep.* **12**, 1–13 (2022).
53. Carolin, S. A. *et al.* Varied response of western Pacific hydrology to climate forcings over the last glacial period. *Science* **340**, 1564–1566 (2013).
54. Cheng, H. *et al.* The climatic cyclicity in semiarid-arid central Asia over the past 500,000 years. *Geophys. Res. Lett.* **39** (2012).
55. Cheng, H. *et al.* The Asian monsoon over the past 640,000 years and ice age terminations. *Nature* **534**, 640–646 (2016).
56. Cheng, H. *et al.* Climate variations of Central Asia on orbital to millennial timescales. *Sci. Rep.* **6**, 1–11 (2016).
57. Clemens, S. *et al.* Precession-band variance missing from East Asian monsoon runoff. *Nat. Commun.* **9**, 1–12 (2018).
58. Clemens, S. C. *et al.* Remote and local drivers of Pleistocene South Asian summer monsoon precipitation: A test for future predictions. *Sci. Adv.*7, eabg3848 (2021).
59. Cruz, F. W. *et al.* Insolation-driven changes in atmospheric circulation over the past 116,000 years in subtropical Brazil. *Nature* **434**, 63–66 (2005).
60. Davtian, N., Bard, E., Darfeuil, S., Ménot, G. & Rostek, F. The novel hydroxylated tetraether index RI-OH' as a sea surface temperature proxy for the 160-45 ka BP period off the Iberian margin. *Paleoceanogr. Paleoclimatol.* **36**, e2020PA004077 (2021).
61. de Abreu, L., Shackleton, N. J., Schönfeld, J., Hall, M. & Chapman, M. Millennial-scale oceanic climate variability off the Western Iberian margin during the last two glacial periods. *Mar. Geol.* **196**, 1–20 (2003).
62. De Deckker, P. *et al.* Climatic evolution in the Australian region over the last 94 ka-spanning human occupancy-, and unveiling the Last Glacial Maximum. *Quat. Sci. Rev.* **249**, 106593 (2020).
63. Denniston, R. F. *et al.* North Atlantic forcing of millennial-scale Indo-Australian monsoon dynamics during the Last Glacial period. *Quat. Sci. Rev.* **72**, 159–168 (2013).
64. Deplazes, G. *et al.* Links between tropical rainfall and North Atlantic climate during the last glacial period. *Nat. Geosci.* **6**, 213–217 (2013).
65. Deplazes, G. *et al.* Weakening and strengthening of the Indian monsoon during Heinrich events and Dansgaard-Oeschger oscillations. *Paleoceanography* **29**, 99–114 (2014).
66. De Pol-Holz, R. *et al.* Late Quaternary variability of sedimentary nitrogen isotopes in the eastern South Pacific Ocean. *Paleoceanography***22** (2007).
67. Dickson, A. J., Austin, W. E., Hall, I. R., Maslin, M. A. & Kucera, M. Centennial-scale evolution of Dansgaard-Oeschger events in the northeast Atlantic Ocean between 39.5 and 56.5 ka BP. *Paleoceanography* **23** (2008).
68. Ding, Z. L. *et al.* Stacked 2.6-Ma grain size record from the Chinese loess based on five sections and correlation with the deep-sea δ18O record. *Paleoceanography* **17**, 5–1 (2002).
69. Dokken, T. M. & Jansen, E. Rapid changes in the mechanism of ocean convection during the last glacial period. *Nature* **401**, 458–461 (1999).
70. Donders, T. *et al.* 1.36 million years of Mediterranean forest refugium dynamics in response to glacial–interglacial cycle strength. *Proc. Natl. Acad. Sci.* **118** (2021).
71. Ehrmann, W. & Schmiedl, G. Nature and dynamics of North African humid and dry periods during the last 200,000 years documented in the clay fraction of Eastern Mediterranean deep-sea sediments. *Quat. Sci. Rev.* **260**, 106925 (2021).
72. Elderfield, H. *et al.* Evolution of ocean temperature and ice volume through the mid-Pleistocene climate transition. *Science* **337**, 704–709 (2012).
73. Erhardt, T. *et al.* Decadal-scale progression of the onset of Dansgaard–Oeschger warming events. *Clim. Past* **15**, 811–825 (2019).
74. Extier, T. *et al.* On the use of δ18Oatm for ice core dating. *Quat. Sci. Rev.* **185**, 244–257 (2018).
75. Eynaud, F. *et al.* Position of the Polar Front along the western Iberian margin during key cold episodes of the last 45 ka. *Geochem. Geophys. Geosyst.* **10** (2009).
76. Fleitmann, D. *et al.* Timing and climatic impact of Greenland interstadials recorded in stalagmites from northern Turkey. *Geophys. Res. Lett.* **36** (2009).
77. Follieri, M., Magri, D. & Sadori, L. Pollen stratigraphical synthesis from Valle di Castiglione (Roma). *Quat. Int.* **3**, 81–84 (1989).
78. Francke, A. *et al.* Sedimentological processes and environmental variability at Lake Ohrid (Macedonia, Albania) between 637 ka and the present. *Biogeosciences* **13**, 1179–1196 (2016).
79. Fritz, S. C. *et al.* Quaternary glaciation and hydrologic variation in the South American tropics as reconstructed from the Lake Titicaca drilling project. *Quat. Res.* **68**, 410–420 (2007).
80. Fritz, S. C., Baker, P., Ekdahl, E., Seltzer, G. & Stevens, L. Millennial-scale climate variability during the Last Glacial period in the tropical Andes. *Quat. Sci. Rev.* **29**, 1017–1024 (2010).
81. Genty, D. *et al.* Isotopic characterization of rapid climatic events during OIS3 and OIS4 in Villars Cave stalagmites (SW-France) and correlation with Atlantic and Mediterranean pollen records. *Quat. Sci. Rev.* **29**, 2799–2820 (2010).
82. Gkinis, V. *et al.* A 120,000-year long climate record from a NW-Greenland deep ice core at ultra-high resolution. *Sci. Data* **8**, 1–9 (2021).
83. Gottschalk, J., Skinner, L. C. & Waelbroeck, C. Contribution of seasonal sub-Antarctic surface water variability to millennial-scale changes in atmospheric CO2 over the last deglaciation and Marine Isotope Stage 3. *Earth Planet. Sci. Lett.* **411**, 87–99 (2015).
84. Grimm, E. C. *et al.* Evidence for warm wet Heinrich events in Florida. *Quat. Sci. Rev.* **25**, 2197–2211 (2006).
85. Hao, Q. *et al.* Delayed build-up of Arctic ice sheets during 400,000-year minima in insolation variability. *Nature* **490**, 393–396 (2012).
86. Harada, N. *et al.* Rapid fluctuation of alkenone temperature in the southwestern Okhotsk Sea during the past 120 ky. *Global Planet. Change* **53**, 29–46 (2006).
87. Hendy, I. L. & Kennett, J. P. Latest Quaternary North Pacific surface-water responses imply atmosphere-driven climate instability. *Geology* **27**, 291–294 (1999).

88. Hendy, I. L., Kennett, J. P., Roark, E. & Ingram, B. L. Apparent synchroneity of submillennial scale climate events between Greenland and Santa Barbara Basin, California from 30–10 ka. *Quat. Sci. Rev.* **21**, 1167–1184 (2002).
89. Hendy, I. L. & Kennett, J. P. Tropical forcing of North Pacific intermediate water distribution during Late Quaternary rapid climate change?. *Quat. Sci. Rev.* **22**, 673–689 (2003).
90. Hodell, D. A., Venz, K. A., Charles, C. D. & Ninnemann, U. S. Pleistocene vertical carbon isotope and carbonate gradients in the South Atlantic sector of the Southern Ocean. *Geochem. Geophys. Geosyst.* **4**, 1–19 (2003).
91. Hodell, D. A., Channell, J. E., Curtis, J. H., Romero, O. E. & Röhl, U. Onset of "Hudson Strait" Heinrich events in the eastern North Atlantic at the end of the middle Pleistocene transition (640 ka)? *Paleoceanography* **23** (2008).
92. Hodell, D. A., Evans, H. F., Channell, J. E. & Curtis, J. H. Phase relationships of North Atlantic ice-rafted debris and surface-deep climate proxies during the last glacial period. *Quat. Sci. Rev.* **29**, 3875–3886 (2010).
93. Hodell, D. *et al.* Response of Iberian Margin sediments to orbital and suborbital forcing over the past 420 ka. *Paleoceanography* **28**, 185–199 (2013).
94. Hodell, D. *et al.* A reference time scale for Site U1385 (Shackleton Site) on the SW Iberian Margin. *Global Planet. Change* **133**, 49–64 (2015).
95. Hodell, D. A. & Channell, J. E. Mode transitions in Northern Hemisphere glaciation: co-evolution of millennial and orbital variability in Quaternary climate. *Clim. Past* **12**, 1805–1828 (2016).
96. Huntley, B., Watts, W., Allen, J. & Zolitschka, B. Palaeoclimate, chronology and vegetation history of the Weichselian Lateglacial: comparative analysis of data from three cores at Lago Grande di Monticchio, southern Italy. *Quat. Sci. Rev.* **18**, 945–960 (1999).
97. Johnson, T. C. *et al.* A progressively wetter climate in southern East Africa over the past 1.3 million years. *Nature* **537**, 220–224 (2016).
98. Jouzel, J. *et al.* Orbital and millennial Antarctic climate variability over the past 800,000 years. *Science* **317**, 793–796 (2007).
99. Jung, S. J., Kroon, D., Ganssen, G., Peeters, F. & Ganeshram, R. Enhanced Arabian Sea intermediate water flow during glacial North Atlantic cold phases. *Earth Planet. Sci. Lett.* **280**, 220–228 (2009).
100. Kanner, L. C., Burns, S. J., Cheng, H. & Edwards, R. L. High-latitude forcing of the South American summer monsoon during the last glacial. *Science* **335**, 570–573 (2012).
101. Kathayat, G. *et al.* Indian monsoon variability on millennial-orbital timescales. *Sci. Rep.* **6**, 1–7 (2016).
102. Kelly, M. J. *et al.* High resolution characterization of the Asian Monsoon between 146,000 and 99,000 years BP from Dongge Cave, China and global correlation of events surrounding Termination II. *Palaeogeogr. Palaeoclimatol. Palaeoecol.* **236**, 20–38 (2006).
103. Lachniet, M. S. *et al.* Late Quaternary moisture export across Central America and to Greenland: evidence for tropical rainfall variability from Costa Rican stalagmites. *Quat. Sci. Rev.* **28**, 3348–3360 (2009).
104. Lachniet, M. S., Denniston, R. F., Asmerom, Y. & Polyak, V. J. Orbital control of western North America atmospheric circulation and climate over two glacial cycles. *Nat. Commun.* **5**, 1–8 (2014).
105. Lambert, F. *et al.* Dust-climate couplings over the past 800,000 years from the EPICA Dome C ice core. *Nature* **452**, 616–619 (2008).
106. Lambert, F., Bigler, M., Steffensen, J. P., Hutterli, M. & Fischer, H. Centennial mineral dust variability in high-resolution ice core data from Dome C. Antarctica. *Clim. Past* **8**, 609–623 (2012).
107. Lauterbach, S. *et al.* An 130 kyr record of surface water temperature and δ18O from the northern Bay of Bengal: Investigating the linkage between Heinrich events and Weak Monsoon Intervals in Asia. *Paleoceanogr. Paleoclimatol.* **35**, e2019PA003646 (2020).
108. Lea, D. W. *et al.* Paleoclimate history of Galápagos surface waters over the last 135,000 yr. *Quat. Sci. Rev.* **25**, 1152–1167 (2006).
109. Loulergue, L. *et al.* Orbital and millennial-scale features of atmospheric CH4 over the past 800,000 years. *Nature* **453**, 383–386 (2008).
110. Lüthi, D. *et al.* High-resolution carbon dioxide concentration record 650,000–800,000 years before present. *Nature* **453**, 379–382 (2008).
111. Martrat, B. *et al.* Four climate cycles of recurring deep and surface water destabilizations on the Iberian margin. *Science* **317**, 502–507 (2007).
112. Melles, M. *et al.* 2.8 million years of Arctic climate change from Lake El'gygytgyn, NE Russia. *Science* **337**, 315–320 (2012).
113. Meyer-Jacob, C. *et al.* Biogeochemical variability during the past 3.6 million years recorded by FTIR spectroscopy in the sediment record of Lake El'gygytgyn, Far East Russian Arctic. *Clim. Past* **10**, 209–220 (2014).
114. Miebach, A., Stolzenberger, S., Wacker, L., Hense, A. & Litt, T. A new Dead Sea pollen record reveals the last glacial paleoenvironment of the southern Levant. *Quat. Sci. Rev.* **214**, 98–116 (2019).
115. Mohtadi, M. *et al.* North Atlantic forcing of tropical Indian Ocean climate. *Nature* **509**, 76–80 (2014).
116. Moine, O. *et al.* The impact of Last Glacial climate variability in west-European loess revealed by radiocarbon dating of fossil earthworm granules. *Proc. Natl. Acad. Sci.* **114**, 6209–6214 (2017).
117. Mosblech, N. A. *et al.* North Atlantic forcing of Amazonian precipitation during the last ice age. *Nat. Geosci.* **5**, 817–820 (2012).
118. Moseley, G. E. *et al.* NALPS19: sub-orbital-scale climate variability recorded in northern Alpine speleothems during the last glacial period. *Clim. Past* **16**, 29–50 (2020).
119. Müller, U. C., Pross, J. & Bibus, E. Vegetation response to rapid climate change in Central Europe during the past 140,000 yr based on evidence from the Füramoos pollen record. *Quat. Res.* **59**, 235–245 (2003).
120. Naafs, B., Hefter, J. & Stein, R. Millennial-scale ice rafting events and Hudson Strait Heinrich (-like) Events during the late Pliocene and Pleistocene: a review. *Quat. Sci. Rev.* **80**, 1–28 (2013).
121. Naafs, B. D. A., Voelker, A., Karas, C., Andersen, N. & Sierro, F. Repeated near-collapse of the Pliocene sea surface temperature gradient in the North Atlantic. *Paleoceanogr. Paleoclimatol.* **35**, e2020PA003905 (2020).
122. Naughton, F. *et al.* Wet to dry climatic trend in north-western Iberia within Heinrich events. *Earth Planet. Sci. Lett.* **284**, 329–342 (2009).
123. Nürnberg, D., Ziegler, M., Karas, C., Tiedemann, R. & Schmidt, M. W. Interacting Loop Current variability and Mississippi River discharge over the past 400 kyr. *Earth Planet. Sci. Lett.* **272**, 278–289 (2008).
124. Pahnke, K., Zahn, R., Elderfield, H. & Schulz, M. 340,000-year centennial-scale marine record of Southern Hemisphere climatic oscillation. *Science* **301**, 948–952 (2003).
125. Petit, J.-R. *et al.* Climate and atmospheric history of the past 420,000 years from the Vostok ice core, Antarctica. *Nature* **399**, 429–436 (1999).
126. Pichevin, L., Bard, E., Martinez, P. & Billy, I. Evidence of ventilation changes in the Arabian Sea during the late Quaternary: Implication for denitrification and nitrous oxide emission. *Global Biogeochem. Cycles***21** (2007).
127. Pickarski, N. & Litt, T. A new high-resolution pollen sequence at Lake Van, Turkey: insights into penultimate interglacial-glacial climate change on vegetation history. *Clim. Past* **13**, 689–710 (2017).
128. Prokopenko, A. A., Hinnov, L. A., Williams, D. F. & Kuzmin, M. I. Orbital forcing of continental climate during the Pleistocene: a complete astronomically tuned climatic record from Lake Baikal, SE Siberia. *Quat. Sci. Rev.* **25**, 3431–3457 (2006).
129. Rampen, S. W. *et al.* Long chain 1, 13-and 1, 15-diols as a potential proxy for palaeotemperature reconstruction. *Geochim. Cosmochim. Acta* **84**, 204–216 (2012).

130. Rasmussen, S. O. *et al.* A first chronology for the North Greenland Eemian Ice Drilling (NEEM) ice core. *Clim. Past* **9**, 2713–2730 (2013).
131. Rasmussen, S. O. *et al.* A stratigraphic framework for abrupt climatic changes during the Last Glacial period based on three synchronized Greenland ice-core records: refining and extending the INTIMATE event stratigraphy. *Quat. Sci. Rev.* **106**, 14–28 (2014).
132. Reille, M. & De Beaulieu, J. Pollen analysis of a long upper Pleistocene continental sequence in a Velay maar (Massif Central, France). *Palaeogeogr. Palaeoclimatol. Palaeoecol.* **80**, 35–48 (1990).
133. Rickaby, R. E. M. & Elderfield, H. Planktonic foraminiferal Cd/Ca: paleonutrients or paleotemperature?. *Paleoceanography* **14**, 293–303 (1999).
134. Riveiros, N. V. *et al.* Response of South Atlantic deep waters to deglacial warming during Terminations V and I. *Earth Planet. Sci. Lett.* **298**, 323–333 (2010).
135. Rosenthal, Y., Oppo, D. W. & Linsley, B. K. The amplitude and phasing of climate change during the last deglaciation in the Sulu Sea, western equatorial Pacific. *Geophys. Res. Lett.* **30** (2003).
136. Rousseau, D.-D. *et al.* (MIS3 & 2) millennial oscillations in Greenland dust and Eurasian aeolian records-A paleosol perspective. *Quat. Sci. Rev.* **169**, 99–113 (2017).
137. Sadori, L. *et al.* Pollen-based paleoenvironmental and paleoclimatic change at Lake Ohrid (south-eastern Europe) during the past 500 ka. *Biogeosciences* **13**, 1423–1437 (2016).
138. Saikku, R., Stott, L. & Thunell, R. A bi-polar signal recorded in the western tropical Pacific: Northern and Southern Hemisphere climate records from the Pacific warm pool during the last Ice Age. *Quat. Sci. Rev.* **28**, 2374–2385 (2009).
139. Salgueiro, E. *et al.* Past circulation along the western Iberian margin: a time slice vision from the Last Glacial to the Holocene. *Quat. Sci. Rev.* **106**, 316–329 (2014).
140. Schulz, H., von Rad, U. & Erlenkeuser, H. Correlation between Arabian Sea and Greenland climate oscillations of the past 110,000 years. *Nature* **393**, 54–57 (1998).
141. Seelos, K., Sirocko, F. & Dietrich, S. A continuous high-resolution dust record for the reconstruction of wind systems in central Europe (Eifel, Western Germany) over the past 133 ka. *Geophys. Res. Lett.* **36** (2009).
142. Stott, L., Poulsen, C., Lund, S. & Thunell, R. Super ENSO and global climate oscillations at millennial time scales. *Science* **297**, 222–226 (2002).
143. Stríkis, N. M. *et al.* South American monsoon response to iceberg discharge in the North Atlantic. *Proc. Natl. Acad. Sci.* **115**, 3788–3793 (2018).
144. Sun, Y., Wang, X., Liu, Q. & Clemens, S. C. Impacts of post-depositional processes on rapid monsoon signals recorded by the last glacial loess deposits of northern China. *Earth Planet. Sci. Lett.* **289**, 171–179 (2010).
145. Sun, Y. *et al.* Influence of Atlantic meridional overturning circulation on the East Asian winter monsoon. *Nat. Geosci.* **5**, 46–49 (2012).
146. Sun, Y. *et al.* Astronomical and glacial forcing of East Asian summer monsoon variability. *Quat. Sci. Rev.* **115**, 132–142 (2015).
147. Sun, Y. *et al.* High-sedimentation-rate loess records: A new window into understanding orbital-and millennial-scale monsoon variability. *Earth Sci. Rev.* **220**, 103731 (2021).
148. Tierney, J. E. *et al.* Northern hemisphere controls on tropical southeast African climate during the past 60,000 years. *Science* **322**, 252–255 (2008).
149. Tzedakis, P. *et al.* Ecological thresholds and patterns of millennial-scale climate variability: The response of vegetation in Greece during the last glacial period. *Geology* **32**, 109–112 (2004).
150. Tzedakis, P., Hooghiemstra, H., Pälike, H., revised chronostratigraphy and long-term vegetation trends. The last 1.35 million years at Tenaghi Philippon. *Quat. Sci. Rev.* **25**, 3416–3430 (2006).
151. Uemura, R. *et al.* Asynchrony between Antarctic temperature and CO2 associated with obliquity over the past 720,000 years. *Nat. Commun.* **9**, 1–11 (2018).
152. Újvári, G. *et al.* AMS 14C and OSL/IRSL dating of the Dunaszekcső loess sequence (Hungary): chronology for 20 to 150 ka and implications for establishing reliable age-depth models for the last 40 ka. *Quat. Sci. Rev.* **106**, 140–154 (2014).
153. Ünal-İmer, E. *et al.* An 80 kyr-long continuous speleothem record from Dim Cave, SW Turkey with paleoclimatic implications for the Eastern Mediterranean. *Sci. Rep.* **5**, 1–11 (2015).
154. Vallelonga, P. *et al.* Iron fluxes to Talos Dome, Antarctica, over the past 200 kyr. *Clim. Past* **9**, 597–604 (2013).
155. Van Kreveld, S. *et al.* Potential links between surging ice sheets, circulation changes, and the Dansgaard-Oeschger cycles in the Irminger Sea, 60–18 kyr. *Paleoceanography* **15**, 425–442 (2000).
156. Veres, D. *et al.* Climate-driven changes in lake conditions during late MIS 3 and MIS 2: a high-resolution geochemical record from Les Echets, France. *Boreas* **38**, 230–243 (2009).
157. Voelker, A. H. *et al.* Mediterranean outflow strengthening during northern hemisphere coolings: a salt source for the glacial Atlantic?. *Earth Planet. Sci. Lett.* **245**, 39–55 (2006).
158. Voelker, A. H. & Abreu, L. d. A review of abrupt climate change events in the Northeastern Atlantic Ocean (Iberian Margin): latitudinal, longitudinal and vertical gradients. *AGU Geophys. Monogr.* (2010).
159. Waelbroeck, C. *et al.* Consistently dated Atlantic sediment cores over the last 40 thousand years. *Sci. Data* **6**, 1–12 (2019).
160. Wagner, J. D. *et al.* Moisture variability in the southwestern United States linked to abrupt glacial climate change. *Nat. Geosci.* **3**, 110–113 (2010).
161. Wagner, B. *et al.* Mediterranean winter rainfall in phase with African monsoons during the past 1.36 million years. *Nature* **573**, 256–260 (2019).
162. WAIS Divide Project Members. Precise interpolar phasing of abrupt climate change during the last ice age. *Nature* **520**, 661–665 (2015).
163. Wang, Y.-J. *et al.* A high-resolution absolute-dated late Pleistocene monsoon record from Hulu Cave, China. *Science* **294**, 2345–2348 (2001).
164. Wang, Y. *et al.* Millennial-and orbital-scale changes in the East Asian monsoon over the past 224,000 years. *Nature* **451**, 1090–1093 (2008).
165. Wang, X. *et al.* Hydroclimate changes across the Amazon lowlands over the past 45,000 years. *Nature* **541**, 204–207 (2017).
166. Weijers, J. W., Schouten, S., Schefuß, E., Schneider, R. R. & Damste, J. S. S. Disentangling marine, soil and plant organic carbon contributions to continental margin sediments: a multi-proxy approach in a 20,000 year sediment record from the Congo deep-sea fan. *Geochim. Cosmochim. Acta* **73**, 119–132 (2009).
167. Weldeab, S., Emeis, K.-C., Hemleben, C., Schmiedl, G. & Schulz, H. Spatial productivity variations during formation of sapropels S5 and S6 in the Mediterranean Sea: evidence from Ba contents. *Palaeogeogr. Palaeoclimatol. Palaeoecol.* **191**, 169–190 (2003).
168. Weldeab, S., Lea, D. W., Schneider, R. R. & Andersen, N. 155,000 years of West African monsoon and ocean thermal evolution. *Science* **316**, 1303–1307 (2007).
169. Whittaker, T. E., Hendy, C. H. & Hellstrom, J. C. Abrupt millennial-scale changes in intensity of Southern Hemisphere westerly winds during marine isotope stages 2–4. *Geology* **39**, 455–458 (2011).
170. Yang, S. & Ding, Z. A 249 kyr stack of eight loess grain size records from northern China documenting millennial-scale climate variability. *Geochem. Geophys. Geosyst.* **15**, 798–814 (2014).

171. Zarriess, M. & Mackensen, A. The tropical rainbelt and productivity changes off northwest Africa: A 31,000-year high-resolution record. *Mar. Micropaleontol.* **76**, 76–91 (2010).
172. Zarriess, M. *et al.* Bipolar seesaw in the northeastern tropical atlantic during heinrich stadials. *Geophys. Res. Lett.* **38** (2011).
173. Zhao, M., Beveridge, N., Shackleton, N., Sarnthein, M. & Eglinton, G. Molecular stratigraphy of cores off northwest Africa: Sea surface temperature history over the last 80 ka. *Paleoceanography* **10**, 661–675 (1995).
174. Ziegler, M., Diz, P., Hall, I. R. & Zahn, R. Millennial-scale changes in atmospheric CO2 levels linked to the Southern Ocean carbon isotope gradient and dust flux. *Nat. Geosci.* **6**, 457–461 (2013).
175. Amante, C. & Eakins, B. W. *ETOPO1 1 Arc-Minute Global Relief Model: Procedures, Data Sources and Analysis*. NOAA Technical Memorandum NESDIS NGDC-24 (National Geophysical Data Center, NOAA, 2009).
176. Massey, F. J. Jr. The Kolmogorov-Smirnov test for goodness of fit. *J. Am. Stat. Assoc.* **46**, 68–78 (1951).
177. Conover, W. J. *Practical Nonparametric Statistics* (Wiley, 1999).
178. Fawcett, T. An introduction to ROC analysis. *Pattern Recogn. Lett.* **27**, 861–874 (2006).
179. Hastie, T., Tibshirani, R. & Friedman, J. *The Elements of Statistical Learning: Data Mining, Inference, and Prediction* (Springer, 2009).
180. Marwan, N., Schinkel, S. & Kurths, J. Recurrence plots 25 years later–Gaining confidence in dynamical transitions. *Europhys. Lett.* **101**, 20007 (2013).
181. Ghil, M., Chekroun, M. D. & Simonnet, E. Climate dynamics and fluid mechanics: natural variability and related uncertainties. *Physica D* **237**, 2111–2126 (2008).
182. Chekroun, M. D., Simonnet, E. & Ghil, M. Stochastic climate dynamics: random attractors and time-dependent invariant measures. *Physica D* **240**, 1685–1700 (2011).
183. Bódai, T. & Tél, T. Annual variability in a conceptual climate model: Snapshot attractors, hysteresis in extreme events, and climate sensitivity. *Chaos* **22**, 023110 (2012).
184. Ghil, M. A century of nonlinearity in the geosciences. *Earth Space Sci.* **6**, 1007–1042 (2019).
185. Riechers, K., Mitsui, T., Boers, N. & Ghil, M. Orbital insolation variations, intrinsic climate variability, and Quaternary glaciations. *Clim. Past* **18**, 863–893 (2022).
186. Bradley, R. S. & Diaz, H. F. Late Quaternary Abrupt Climate Change in the Tropics and Sub-Tropics: The Continental Signal of Tropical Hydroclimatic Events (THEs). *Rev. Geophys.* **59**, e2020RG000732 (2021).
187. Zachos, J., Pagani, M., Sloan, L., Thomas, E. & Billups, K. Trends, rhythms, and aberrations in global climate 65 Ma to present. *Science* **292**, 686–693 (2001).
188. Coxall, H. K., Wilson, P. A., Pälike, H., Lear, C. H. & Backman, J. Rapid stepwise onset of Antarctic glaciation and deeper calcite compensation in the Pacific Ocean. *Nature* **433**, 53–57 (2005).
189. Rousseau, D.-D., Bagniewski, W. & Lucarini, V. A Punctuated Equilibrium Analysis of the Climate Evolution of Cenozoic: Hierarchy of Abrupt Transitions. *Res. Sq.*https://doi.org/10.21203/rs.3.rs-2359196/v1 *(2022).*
190. Miller, K. G., Fairbanks, R. G. & Mountain, G. S. Tertiary oxygen isotope synthesis, sea level history, and continental margin erosion. *Paleoceanography* **2**, 1–19 (1987).
191. Flower, B. P. & Kennett, J. P. The middle Miocene climatic transition: East Antarctic ice sheet development, deep ocean circulation and global carbon cycling. *Palaeogeogr. Palaeoclimatol. Palaeoecol.* **108**, 537–555 (1994).
192. Miller, K. *et al.* Cenozoic sea-level and cryospheric evolution from deep-sea geochemical and continental margin records. *Sci. Adv.* **6**, 1346 (2020).
193. Rohling, E. *et al.* Sea level and deepsea temperature reconstructions suggest quasi-stable states and critical transitions over the past 40 million years. *Sci. Adv.* **7**, 5326 (2021).
194. Emiliani, C. & Geiss, J. On glaciations and their causes. *Geol. Rundsch.* **46**, 576–601 (1959).
195. Boers, N., Marwan, N., Barbosa, H. M. J. & Kurths, J. A deforestation-induced tipping point for the South American monsoon system. *Sci. Rep.* **7** (2017).
196. Ruddiman, W. F. North Atlantic ice-rafting: a major change at 75,000 years before the present. *Science* **196**, 1208–1211 (1977).
197. Rousseau, D.-D., Bagniewski, W. & Ghil, M. Abrupt climate changes and the astronomical theory: are they related?. *Clim. Past* **18**, 249–271 (2022).
198. Lisiecki, L. E. & Raymo, M. E. A Pliocene-Pleistocene stack of 57 globally distributed benthic δ18O records. *Paleoceanography* **20** (2005).
199. Miller, K. G., Wright, J. D. & Fairbanks, R. G. Unlocking the ice house: Oligocene-Miocene oxygen isotopes, eustasy, and margin erosion. *J. Geophys. Res. Solid Earth* **96**, 6829–6848 (1991).
200. Boulila, S. *et al.* On the origin of Cenozoic and Mesozoic "third-order" eustatic sequences. *Earth Sci. Rev.* **109**, 94–112 (2011).
201. Shackleton, N. J., Hall, M. A., Raffi, I., Tauxe, L. & Zachos, J. Astronomical calibration age for the Oligocene-Miocene boundary. *Geology* **28**, 447–450 (2000).
202. Pinero, E., Marquardt, M., Hensen, C., Haeckel, M. & Wallmann, K. Estimation of the global inventory of methane hydrates in marine sediments using transfer functions. *Biogeosciences* **10**, 959–975 (2013).
203. Dansgaard, W. *et al.* Evidence for general instability of past climate from a 250-kyr ice-core record. *Nature* **364**, 218–220 (1993).
204. Schneider, S. H. & Dickinson, R. E. Climate modeling. *Rev. Geophys.* **12**, 447–493 (1974).
205. Buizert, C. *et al.* Abrupt ice-age shifts in southern westerly winds and Antarctic climate forced from the north. *Nature* **563**, 681–685 (2018).
206. Adolphi, F. *et al.* Connecting the Greenland ice-core and U/ Th timescales via cosmogenic radionuclides: testing the synchroneity of Dansgaard-Oeschger events. *Clim. Past* **14**, 1755–1781 (2018).
207. Comas-Bru, L. *et al.* SISALv2: a comprehensive speleothem isotope database with multiple age-depth models. *Earth Syst. Sci. Data* **12**, 2579–2606 (2020).
208. Lee, T., Rand, D., Lisiecki, L. E., Gebbie, G. & Lawrence, C. E. Bayesian age models and stacks: Combining age inferences from radiocarbon and benthic δ18O stratigraphic alignment. *EGUsphere* 1–29 (2022).

Acknowledgements

We would like to express our gratitude to two anonymous reviewers whose thoughtful and constructive comments significantly improved the overall quality of the paper. This work is Tipping Points in the Earth System (TiPES) contribution #180. This study has been funded by the European Union's Horizon 2020 research and innovation programme (grant agreement No. 820970). This is LDEO contribution.

Author contributions

W.B., D.D.R. and M.G.. outlined the manuscript, W.B. and D.D.R. collected the datasets, W.B. carried out the computations and drew the plots, and W.B., D.D.R. and M.G. analyzed the results. W.B. drafted the manuscript and all authors reviewed and finalized it.

Competing interests
The authors declare no competing interests.

Additional information
Supplementary Information The online version contains supplementary material available at https://doi.org/10.1038/s41598-023-30592-1.

Correspondence and requests for materials should be addressed to W.B.

Reprints and permissions information is available at www.nature.com/reprints.

Publisher's note Springer Nature remains neutral with regard to jurisdictional claims in published maps and institutional affiliations.

Supplementary Information for: The PaleoJump database for abrupt transitions in past climates

Witold Bagniewski[1,*], Denis-Didier Rousseau[2,3,4], and Michael Ghil[1,5]

[1]Department of Geosciences and Laboratoire de Météorologie Dynamique (CNRS and IPSL), École Normale Supérieure and PSL University, Paris, France
[2]Geosciences Montpellier, University of Montpellier, CNRS, Montpellier, France
[3]Institute of Physics - CSE, Division of Geochronology and Environmental Isotopes, Silesian University of Technology, Gliwice, Poland
[4]Lamont-Doherty Earth Observatory, Columbia University, New York, USA
[5]Department of Atmospheric and Oceanic Sciences, University of California at Los Angeles, Los Angeles, USA
[*]wbagniewski@lmd.ipsl.fr

ABSTRACT

Tipping points (TPs) in Earth's climate system have been the subject of increasing interest and concern in recent years, given the risk that anthropogenic forcing could cause abrupt, potentially irreversible, climate transitions. Paleoclimate records are essential for identifying past TPs and for gaining a thorough understanding of the underlying nonlinearities and bifurcation mechanisms. However, the quality, resolution, and reliability of these records can vary, making it important to carefully select the ones that provide the most accurate representation of past climates. Moreover, as paleoclimate time series vary in their origin, time spans, and periodicities, an objective, automated methodology is crucial for identifying and comparing TPs. To address these challenges, we introduce the open-source PaleoJump database, which contains a collection of carefully selected, high-resolution records originating in ice cores, marine sediments, speleothems, terrestrial records, and lake sediments. These records describe climate variability on centennial, millennial and longer time scales and cover all the continents and ocean basins. We provide an overview of their spatial distribution and discuss the gaps in coverage. Our statistical methodology includes an augmented Kolmogorov-Smirnov test and Recurrence Quantification Analysis; it is applied here, for illustration purposes, to selected records in which abrupt transitions are automatically detected and the presence of potential tipping elements is investigated. These transitions are shown in the PaleoJump database along with other essential information about the records, including location, temporal scale and resolution, as well as temporal plots. This open-source database represents, therefore, a valuable resource for researchers investigating TPs in past climates.

Supplementary Tables

The sites of proxy records included in the PaleoJump database have been compiled in five tables according to their geological nature. For each site, the available data have been analyzed to determine the essential information, which is given in the tables below: location, depth/elevation, temporal range, maximum temporal resolution, and types of paleoproxies. This information is accompanied by links to the original data and the associated publications. The "maximum resolution" value in the tables is calculated as the maximum of the average temporal resolution for a 10-kyr time interval, excluding the Holocene and the late deglacial, i.e. the last 14 000 years, during which the proxy time resolution is frequently much higher than for the older part of the record. This was done so as to allow a more accurate comparison of the centennial- and millennial-scale variabilities between different records of the glacial and earlier interglacials periods.

1. Records included in the PaleoJump database

Site name	Location	Depth	Age	Res.	Proxies
MD95-2010[1]	66.684, 4.566	1226 m	67 - 10 ka	35 y	pla δ^{18}O; ben δ^{18}O; pla δ^{13}C; ben δ^{13}C; IRD; mag sus
ODP162-983[2]	60.403, -23.641	1984 m	1.2 - 0 Ma	89 y	IRD; %NPS
SO82-5[3,4]	59.186, -30.905	1416 m	57 - 15 ka	62 y	pla δ^{18}O; ben δ^{18}O; pla δ^{13}C; ben δ^{13}C; SST; IRD
MD95-2006[5]	57.03, -10.058	2122 m	56 - 40 ka	90 y	pla δ^{18}O; ben δ^{18}O; pla δ^{13}C; ben δ^{13}C; %NPS; SST; IRD
JPC-13[6]	53.057, -33.53	3082 m	128 - 7 ka	12 y	pla δ^{18}O; pla δ^{13}C; ben δ^{18}O; ben δ^{13}C; grain size; XRF
U1308[7,8]	49.878, -24.238	3871 m	3.14 - 0 Ma	118 y	ben δ^{18}O; ben δ^{13}C; bulk carbonate δ^{18}O; Ca/Sr; Si/Sr; pla δ^{18}O
MD01-2412[9]	44.523, 145.003	1225 m	116 - 0 ka	113 y	SST
MD99-2331[10–13]	42.15, -9.683	2120 m	160 - 16 ka	137 y	pla δ^{18}O; IRD; SST; pollen; temperate forest pollen
U1313[14–16]	41, -32.957	3426 m	4.3 - 0 Ma	185 y	pla δ^{18}O; ben δ^{18}O; SST; Qz/Cal
MD95-2040[17,18]	40.582, -9.861	2465 m	360 - 0 ka	78 y	pla δ^{18}O; pla δ^{13}C; ben δ^{18}O; ben δ^{13}C; SST; IRD
MD95-2039[10,19]	40.579, -10.349	3381 m	51 - 0 ka	107 y	pla δ^{18}O; IRD; SST
MD01-2443[17,20]	37.881, -10.176	2925 m	433 - 86 ka	188 y	pla δ^{18}O; ben δ^{18}O; ben δ^{13}C; SST
MD95-2042[10,11,21,22]	37.8, -10.167	3146 m	418 - 0 ka	83 y	pla δ^{18}O; ben δ^{18}O; ben δ^{13}C; pla δ^{13}C; SST
U1385[23,24]	37.571, -10.126	2587 m	1.4 - 0 Ma	47 y	pla δ^{18}O; reflectance; ben δ^{18}O; SST
MD01-2444[20,21]	37.565, -10.134	2656 m	420 - 0 ka	86 y	pla δ^{18}O; ben δ^{18}O; ben δ^{13}C; reflectance; SST
MD99-2341[10]	36.389, -7.066	582 m	49 - 1 ka	104 y	pla δ^{18}O
ODP977a[21]	36.032, -1.955	1984 m	244 - 0 ka	181 y	SST
MD99-2339[19,25]	35.886, -7.528	1177 m	47 - 0 ka	38 y	pla δ^{18}O; ben δ^{18}O; pla δ^{13}C; ben δ^{13}C; SST; grain size
M40/4_SL71[26–28]	34.811, 23.194	2788 m	182 - 0 ka		grain size; XRF; clay; pla δ^{18}O
ODP893A[29–31]	34.28, -120.03	576 m	65 - 0 ka	41 y	pla δ^{18}O; pla δ^{13}C; ben δ^{18}O
U1429[32]	31.617, 128.998	732 m	393 - 0 ka		pla δ^{18}O; ben δ^{18}O; ben δ^{13}C; pla δ^{13}C; SST
MD02-2575[33]	29.002, -87.119	847 m	400 - 1 ka	135 y	pla δ^{18}O; ben δ^{18}O; SST
MD04-2876[34]	24.843, 64.008	828 m	50 - 0 ka	169 y	δ^{15}N; total N; TOC
SO90-93KL[35]	23.583, 64.217	1802 m	109 - 1 ka	177 y	pla δ^{18}O
SO130-289KL[36,37]	23.122, 66.497	571 m	79 - 2 ka	0.2 y	reflectance; grain size; TOC; ...
SO90-136KL[35]	23.117, 66.5	568 m	66 - 2 ka	63 y	TOC
SO90-111KL[35]	23.1, 66.483	775 m	62 - 2 ka	72 y	TOC
ODP658C[38]	20.75, -18.583	2263 m	84 - 0 ka	135 y	SST
SO188-17286-1[39]	19.743, 89.879	1428 m	129 - 0 ka	158 y	pla δ^{18}O; ben δ^{18}O; SST
U1446[40]	19.083, 85.733	1440 m	1.46 - 0 Ma	24 y	Rb/Ca
GeoB9526-5[41,42]	12.435, -18.057	3223 m	72 - 1 ka	55 y	Fe/K; SST; ben δ^{18}O
NIOP905[43]	10.767, 51.951	1580 m	88 - 1 ka	145 y	ben δ^{18}O; ben δ^{13}C
MD03-2621[36]	10.678, -64.972	847 m	109 - 6 ka	0.1 y	reflectance
MD97-2141[44]	8.78, 121.28	3633 m	395 - 5 ka	51 y	pla δ^{18}O
MD98-2181[45,46]	6.3, 125.83	2114 m	68 - 0 ka	66 y	pla δ^{18}O; pla δ^{13}C; ben δ^{18}O; SST
MD03-2707[47]	2.502, 9.395	1295 m	155 - 0 ka	92 y	pla δ^{18}O; SST; BWT
TR163-22[48]	0.52, -92.4	2830 m	135 - 1 ka	169 y	pla δ^{18}O; ben δ^{18}O; SST
SO189-039KL[49]	-0.79, 99.908	517 m	45 - 0 ka	66 y	pla δ^{18}O; SST

Site name	Location	Depth	Age	Res.	Proxies
GeoB6518-1[50,51]	-5.588, 11.222	962 m	43 - 0 ka		pla δ^{18}O; ben δ^{18}O; TOC; SST
GeoB7139-2[52]	-30.2, -71.983	3267 m	70 - 1 ka	53 y	δ^{15}N; total N
MD03-2611G[53]	-36.73, 136.548	2420 m	94 - 0 ka	15 y	pla δ^{18}O; pla δ^{13}C; SST; quartz; Ti
ODP1089[54]	-40.93, 9.9	4621 m	615 - 0 ka	189 y	pla δ^{18}O; ben δ^{18}O; pla δ^{13}C; ben δ^{13}C
TNO57-21[55]	-41.1, 7.8	4981 m	99 - 0 ka	112 y	pla δ^{18}O; %NPS
MD02-2588[56]	-41.332, 25.828	2907 m	353 - 0 ka	246 y	ben δ^{18}O; ben δ^{13}C; pla δ^{13}C
ODP181-1123[57]	-41.786, -171.499	3290 m	1.5 - 0 Ma	388 y	ben δ^{18}O; ben δ^{13}C; Mg/Ca
MD07-3076Q[58,59]	-44.153, -14.228	3770 m	67 - 1 ka	61 y	pla δ^{18}O; pla δ^{13}C; SST
MD97-2120[60]	-45.534, 174.931	1210 m	151 - 4 ka	103 y	pla δ^{18}O; SST
MD88-770[61]	-46.017, 96.467	3290 m	149 - 5 ka	187 y	SST
CENOGRID stack[62]	N/A	N/A	67.1 - 0 Ma	2000 y	ben δ^{18}O; ben δ^{13}C

Supplementary Table S 1. Marine Sediment Cores, ordered by latitude. Res.: temporal resolution, pla: planktic, ben: benthic, SST: sea surface temperature, BWT: bottom water temperature, IRD: ice rafted detritus, TOC: total organic carbon, mag sus: magnetic susceptibility.

Site name	Location	Elevation	Age	Res.	Proxies
NEEM[63–65]	77.45, -51.06	2545 m	129 - 0 ka	4 y	δ^{18}O; Ca^{2+}; Na+; ...
NGRIP[66,67]	75.1, -42.32	2925 m	122 - 0 ka	20 y	δ^{18}O; Ca; dust; CH4; ...
GISP2[66]	72.97, -38.8	3208 m	104 - 0 ka	20 y	δ^{18}O; Ca^{2+}; CH4; δ^{15}N; ...
GRIP[66]	72.58, -37.63	3200 m	104 - 0 ka	20 y	δ^{18}O; Ca; CH4; ...
Guliya[68]	35.28, 81.48	6200 m	132 - 0 ka	400 y	δ^{18}O; dust; ...
TALDICE[69,70]	-72.783, 159.067	2315 m	314 - 0 ka	39 y	δ^{18}O; CH4; Fe
EPICA EDML[71]	-75.003, 0.068	2416 m	150 - 0 ka	19 y	δ^{18}O
EPICA Dome C[72–77]	-75.1, 123.35	3189 m	802 - 0 ka	39 y	δD; δT; CO2; CH4; dust; δ^{18}O; Ca^{2+}
Dome Fuji[78]	-77.32, 38.7	3810 m	716 - 0 ka	34 y	δ^{18}O; dust
Vostok[79]	-78.47, 106.8	3488 m	423 - 0 ka	55 y	δD; δT; CH4; dust; ...
WAIS Divide[80]	-79.468, -112.087	1806 m	68 - 0 ka	12 y	δ^{18}O; CH4; ...
Synthetic Greenland[81]	N/A	2135 m	798 - 5 ka	50 y	δ^{18}O

Supplementary Table S 2. Ice cores, ordered by latitude.

Site name	Location	Elevation	Age	Res.	Proxies
Gassel Tropfsteinhöhle Cave[82]	47.823, 13.843	1225 m	108 - 77 ka	5 y	δ^{18}O
Grete-Ruth Cave[82]	47.543, 12.027	1435 m	111 - 103 ka	12 y	δ^{18}O
Hölloch im Mahdtal Cave[82]	47.378, 10.151	1438 m	74.4 - 73.6 ka	5 y	δ^{18}O
Schneckenloch Cave[82,83]	47.375, 10.068	1285 m	118 - 64 ka	7 y	δ^{18}O
Grosser Baschg Cave[82,83]	47.25, 9.667	785 m	87 - 81 ka	14 y	δ^{18}O
Villars Cave (Vil-stm09)[84,85]	45.442, 0.785	175 m	83 - 31 ka	88 y	δ^{18}O; δ^{13}C
Kesang Cave[86]	42.93, 81.78	2000 m	500 - 52 ka	23 y	δ^{18}O
Sofular Cave[87]	41.416, 31.934	700 m	50 - 0 ka	18 y	δ^{18}O; δ^{13}C
Tonnel'naya Cave[88]	38.4, 67.23	3226 m	134 - 8 ka	1 y	δ^{18}O; δ^{13}C
Leviathan Cave[89]	37.831, -115.607	2400 m	174 - 0 ka	50 y	δ^{18}O
Dim Cave (Dim-E3)[90]	36.54, 32.109	232 m	90 - 10 ka	82 y	δ^{18}O; δ^{13}C
Devils Hole[91]	36.425, -116.291	719 m	204 - 5 ka	65 y	δ^{18}O; δ^{13}C
Fort Stanton Cave[92]	33.507, -105.494	1864 m	56 - 11 ka	23 y	δ^{18}O
Hulu Cave (MSD; MSL)[93]	32.058,119.041	86 m	76 - 18 ka	68 y	δ^{18}O; U/Th ages
Cave of the Bells[94]	31.729, -110.768	1639 m	53 - 11 ka	18 y	δ^{18}O
Sanbao Cave[95,96]	31.667, 110.433	1900 m	641 - 0 ka		δ^{18}O; U/Th ages

Site name	Location	Elevation	Age	Res.	Proxies
Soreq Cave[97]	31.45, 35.03	400 m	184 - 0 ka	44 y	δ^{18}O; δ^{13}C
Bittoo Cave[98]	30.79, 77.776	3000 m	284 - 0 ka	18 y	δ^{18}O; δ^{13}C
Abaco Island Cave[99]	26.23, -77.16	-17 m	64 - 14 ka	14 y	δ^{18}O; δ^{13}C; Sr/Ca; Mg/Ca
Dongge Cave[100]	25.28, 108.08	680 m	146 - 99 ka	20 y	δ^{18}O; U/Th ages
Moomi Cave[101]	12.533,54.317	400 m	53 - 40 ka	15 y	δ^{18}O
Terciopelo Cave[102]	10.167, -85.333	370 m	98 - 24 ka	100 y	δ^{18}O
Northern Borneo[103]	4.085, 114.85	250 m	162 - 0 ka	55 y	δ^{18}O
Santiago Cave[104]	-3.017, -78.133	980 m	94 - 6 ka	49 y	δ^{18}O
Paraiso Cave (PAR07)[105]	-4.067, -55.45	60 m	45 - 18 ka	21 y	δ^{18}O; δ^{13}C
Pacupahuain Cave[106]	-11.24, -75.82	3800 m	50 - 16 ka	27 y	δ^{18}O; δ^{13}C
Lapa Sem Fim Cave[107]	-16.149, -44.627	690 m	84 - 12 ka	8 y	δ^{18}O
Lapa Grande Cave[107]	-16.707,-43.943	730 m	84 - 40 ka	14 y	δ^{18}O
Ball Gown Cave[108]	-17.28, 125.12	100 m	40 - 8 ka		δ^{18}O
Botuvera Cave[109]	-27.225, -49.158	230 m	116 - 0 ka	95 y	δ^{18}O; δ^{13}C
Hollywood Cave[110]	-41.952, 171.476	130 m	73 - 11 ka	58 y	δ^{18}O; δ^{13}C
China cave composite[96]	N/A	N/A	641 - 0 ka	22 y	δ^{18}O; U/Th ages

Supplementary Table S 3. Speleothems, ordered by latitude.

Site name	Location	Elevation	Age	Res.	Proxies
ELSA-Eifel loess stack[111]	50.16, 6.83	403 m	132 - 0 ka	100 y	dust
Nussloch loess[112,113]	49.316, 8.722	180 m	130 - 18 ka		grain size; δ^{13}C; Snails; earth worms; mag sus; paleosol-loess doublets
Dunaszekcso loess[114]	46.09, 18.763	135 m	150 - 20 ka		grain size; paleosol-loess doublets
Chashmanigar loess	38.392, 69.833	1400 m	1.77 - 0 Ma		grain size; mag sus; reflectance
Gulang loess[115–117]	37.49, 102.88	2400 m	1.48 - 0 Ma	50 y	grain size; δ^{13}C
Jiyuan loess[118]	37.14, 107.39	1730 m	130 - 0 ka		grain size
Zichang loess[118]	37.14, 109.85	1265 m	249 - 0 ka		grain size
Hongde loess[118]	36.77, 107.21	1640 m	249 - 0 ka		grain size
Huanxian loess[118]	36.65, 107.26	1500 m	249 - 0 ka		grain size
Jingyuan loess[115–117,119]	36.35, 104.62	2050 m	1.7 - 0 Ma	26 y	grain size; δ^{13}C
Huachi loess[118]	36.34, 107.93	1395 m	249 - 0 ka		grain size
Xinzhuangyuan loess[118]	36.19, 104.73	2110 m	249 - 0 ka		grain size
Linxia loess[117,118]	36.15, 103.63	2210 m	660 - 0 ka		grain size
Lijiayuan loess[118]	36.12, 104.86	1850 m	249 - 0 ka		grain size
Yimaguan loess[120]	35.917, 107.617	1500 m	879 - 0 ka	197 y	grain size; mag sus
Luochuan loess[120]	35.717, 109.417	1100 m	884 - 0 ka	289 y	grain size; mag sus
Chinese Loess Plateau stack[121]	35.41,107.73	1300 m	3.6 - 0 Ma	1000 y	grain size; mag sus
Chiloparts loess stack[122]	35.3, 107.6	1300 m	2.6 - 0 Ma		grain size
Lingtai loess[119]	35.067, 107.65	1350 m	7 - 0 Ma	107 y	grain size; mag sus; carbonate
CHILOMOS loess stack[118]	N/A	N/A	249 - 0 ka	200 y	grain size

Supplementary Table S 4. Loess and dust records, ordered by latitude.

Site name	Location	Elevation	Age	Res.	Proxies
Lake El'gygytgyn[123,124]	67.5, 172.104	489 m	3.6 - 0 Ma	27 y	Mn/Fe; Si/Ti; mag sus; TOC; TIC; biogenic Si
Lake Baikal[125]	53.696, 108.352	456 m	1.8 - 0 Ma	223 y	biogenic Si
Füramoos[126]	47.983, 9.883	662 m	140 - 0 ka		pollen
Les Echets[127,128]	45.833, 5	267 m	46 - 15 ka		pollen; diatoms; mag sus; geochemistry

Site name	Location	Elevation	Age	Res.	Proxies
Lac du Bouchet[13,129]	44.83, 3.82	1200 m	70 - 0 ka	89 y	pollen; temperate forest pollen
Summer Lake[130]	42.83, -120.75	1260 m	46 - 23 ka	76 y	δ^{18}O; δ^{13}C
Valle di Castiglione[13,131]	41.9, 12.76	44 m	56 - 14 ka	357 y	pollen; temperate forest pollen
Tenaghi Philippon[132]	41.17, 24.33	40 m	1.35 - 0 Ma		pollen
Lake Ohrid[133–136]	41.049, 20.715	693 m	1.36 - 0 Ma	208 y	δ^{18}O; δ^{13}C; TIC; Zr/K; pollen; ...
Lago di Monticchio[137–139]	40.932, 15.605	656 m	100 - 10 ka	120 y	pollen; temperate forest pollen; biogenic Si; dry density
Ioannina[13,140]	39.75, 20.85	470 m	130 - 0 ka	150 y	pollen; temperate forest pollen
Lake Van[141]	38.667, 42.669	1649 m	250 - 129 ka	336 y	δ^{18}O; δ^{13}C; pollen; ...
Padul[142–144]	37, -3.67	785 m	197 - 0 ka	102 y	pollen, precipitation
Dead Sea[145]	31.508, 35.471	-428 m	88 - 14 ka	242 y	pollen
Lake Tulane[146]	27.584, -81.502	36 m	61 - 0 ka		Pinus pollen
Lake Tanganyika[147]	-6.714, 29.833	773 m	59 - 1 ka	260 y	δ^{13}C; δD; Lake Surface Temperature
Lake Malawi[148]	-11.294, 34.437	500 m	1.28 - 0 Ma	14 y	Ca; T; δ^{13}C
Lake Titicaca[149,150]	-15.937, -69.16	3810 m	370 - 3 ka	28 y	TOC; δ^{13}C; grain size

Supplementary Table S 5. Lake sediment cores, ordered by latitude.

Supplementary Figures

CENOGRID stack, including transitions detected using a shorter window length

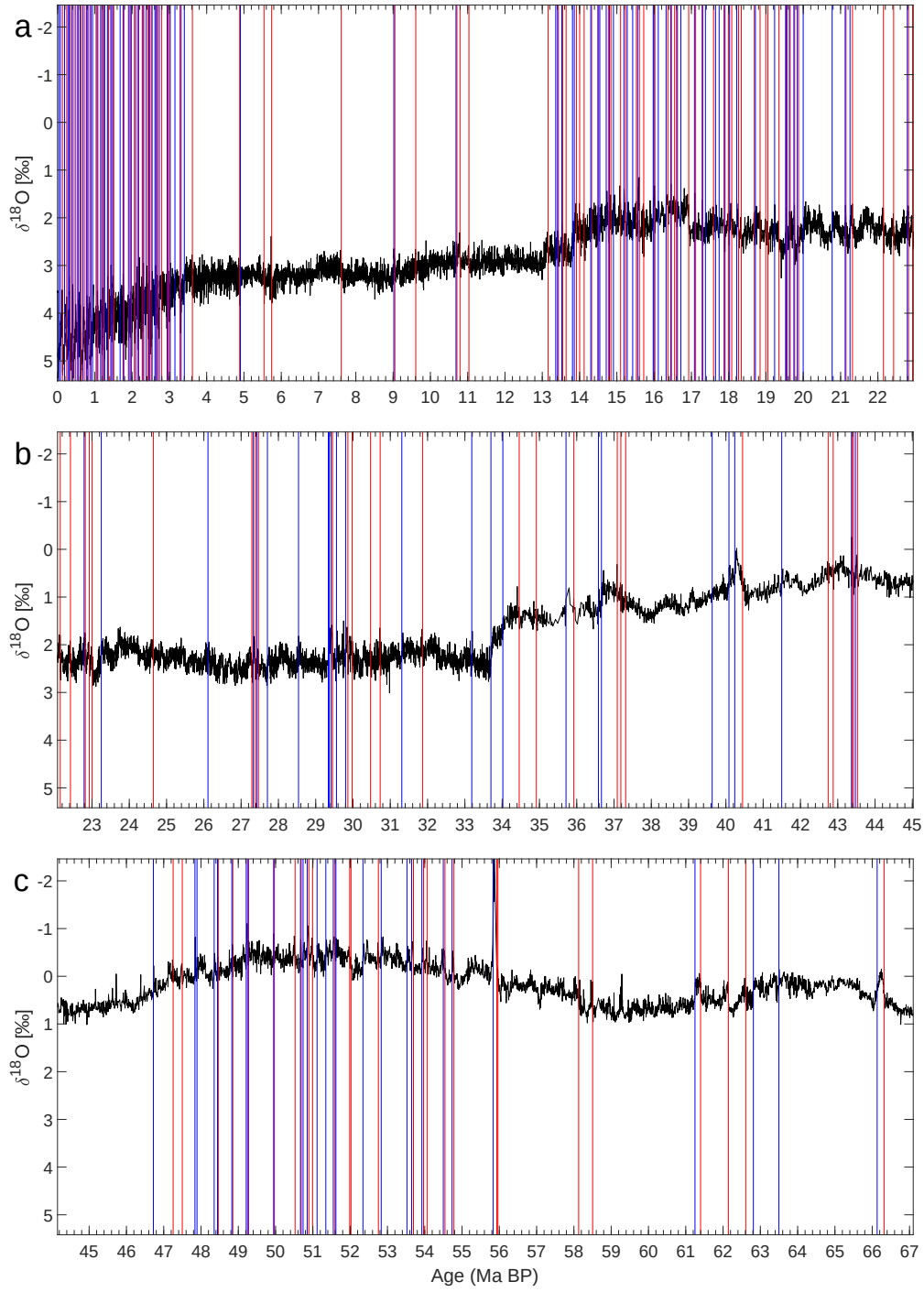

Supplementary Figure S 1. CENOGRID stack of benthic δ^{18}O[62]: (a) 22.9-0 Ma BP; (b) 45-22.1 Ma BP; and (c) 67.1-44.2 Ma BP. Vertical lines represent transitions detected by the KS test[151], with red lines for warming transitions and blue lines for cooling ones. Transitions detected for the entire record using a window length of $0.02 \leq w \leq 2.5$ Myr. The vertical axes are reversed.

U1308 marine sediment core, including detected transitions

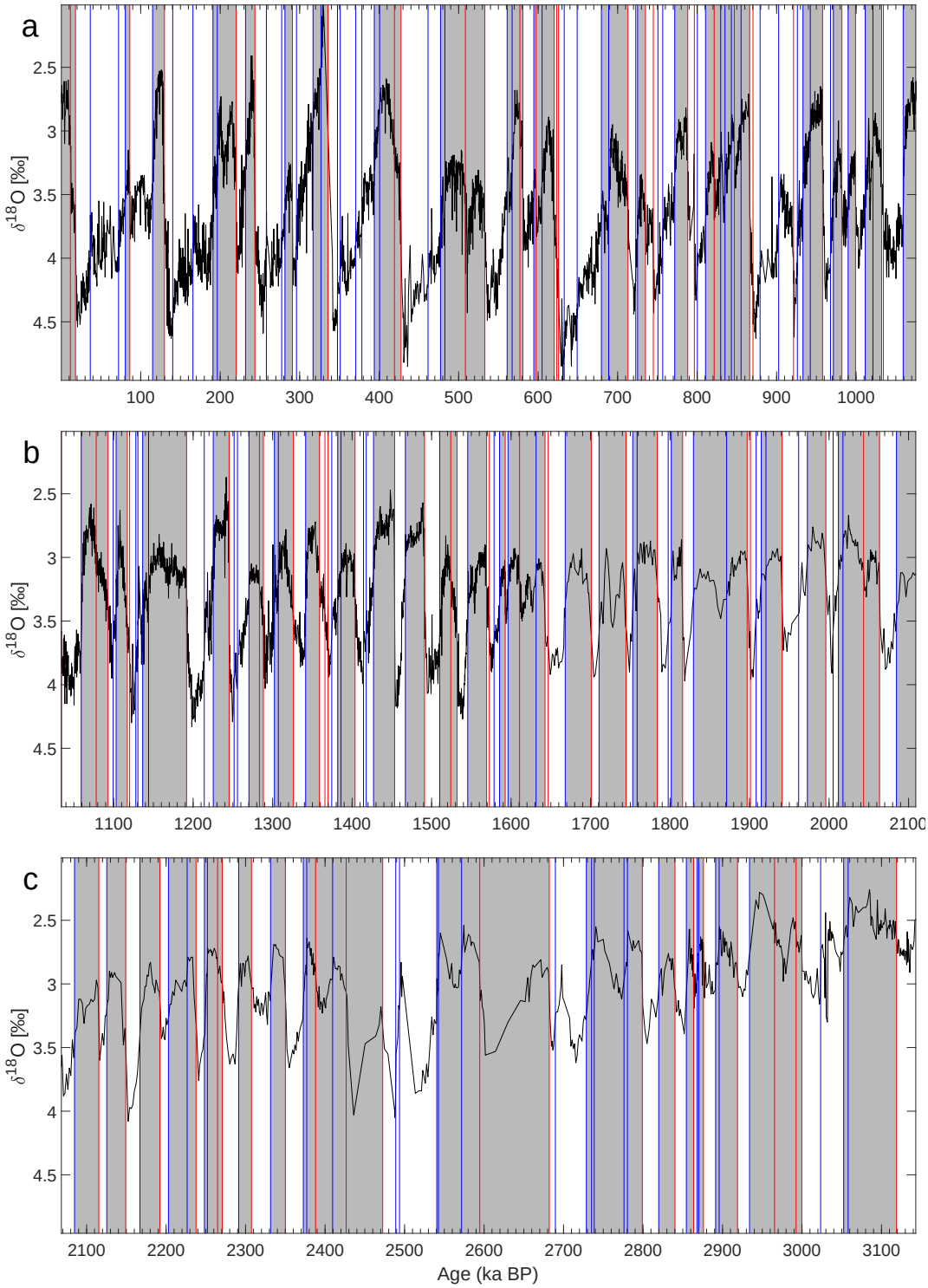

Supplementary Figure S 2. Benthic *Cibicidoides sp.* record in the U1308 marine sediment core δ^{18}O[7]: (a) 1.07-0 Ma BP; (b) 2.11-1.04 Ma BP; and (c) 3.14-2.07 Ma BP. Vertical lines represent transitions detected by the KS test[151], with red lines for warming transitions and blue lines for cooling ones. Vertical axes are reversed. Marine isotope stages (MISs) are shaded, with grey bars representing interglacials (odd-numbered MISs), while white bars represent glacials (even-numbered MISs). See also the analysis of this record by Rousseau et al.[152]

References

1. Dokken, T. M. & Jansen, E. Rapid changes in the mechanism of ocean convection during the last glacial period. *Nature* **401**, 458–461 (1999).
2. Barker, S. *et al.* Early interglacial legacy of deglacial climate instability. *Paleoceanography and Paleoclimatology* **34**, 1455–1475 (2019).
3. Van Kreveld, S. *et al.* Potential links between surging ice sheets, circulation changes, and the Dansgaard-Oeschger cycles in the Irminger Sea, 60–18 kyr. *Paleoceanography* **15**, 425–442 (2000).
4. Waelbroeck, C. *et al.* Consistently dated Atlantic sediment cores over the last 40 thousand years. *Scientific Data* **6**, 1–12 (2019).
5. Dickson, A. J., Austin, W. E., Hall, I. R., Maslin, M. A. & Kucera, M. Centennial-scale evolution of Dansgaard-Oeschger events in the northeast Atlantic Ocean between 39.5 and 56.5 ka BP. *Paleoceanography* **23** (2008).
6. Hodell, D. A., Evans, H. F., Channell, J. E. & Curtis, J. H. Phase relationships of North Atlantic ice-rafted debris and surface-deep climate proxies during the last glacial period. *Quaternary Science Reviews* **29**, 3875–3886 (2010).
7. Hodell, D. A. & Channell, J. E. Mode transitions in Northern Hemisphere glaciation: co-evolution of millennial and orbital variability in Quaternary climate. *Climate of the Past* **12**, 1805–1828 (2016).
8. Hodell, D. A., Channell, J. E., Curtis, J. H., Romero, O. E. & Röhl, U. Onset of "Hudson Strait" Heinrich events in the eastern North Atlantic at the end of the middle Pleistocene transition (~640 ka)? *Paleoceanography* **23** (2008).
9. Harada, N. *et al.* Rapid fluctuation of alkenone temperature in the southwestern Okhotsk Sea during the past 120 ky. *Global and Planetary Change* **53**, 29–46 (2006).
10. Eynaud, F. *et al.* Position of the Polar Front along the western Iberian margin during key cold episodes of the last 45 ka. *Geochemistry, Geophysics, Geosystems* **10** (2009).
11. Davtian, N., Bard, E., Darfeuil, S., Ménot, G. & Rostek, F. The Novel Hydroxylated Tetraether Index RI-OH' as a Sea Surface Temperature Proxy for the 160-45 ka BP Period Off the Iberian Margin. *Paleoceanography and Paleoclimatology* **36**, e2020PA004077 (2021).
12. Naughton, F. *et al.* Wet to dry climatic trend in north-western Iberia within Heinrich events. *Earth and Planetary Science Letters* **284**, 329–342 (2009).
13. Sánchez Goñi, M. F. *et al.* The ACER pollen and charcoal database: a global resource to document vegetation and fire response to abrupt climate changes during the last glacial period. *Earth System Science Data* **9**, 679–695 (2017).
14. Bolton, C. T. *et al.* North Atlantic midlatitude surface-circulation changes through the Plio-Pleistocene intensification of Northern Hemisphere glaciation. *Paleoceanography and Paleoclimatology* **33**, 1186–1205 (2018).
15. Naafs, B. D. A., Voelker, A., Karas, C., Andersen, N. & Sierro, F. Repeated near-collapse of the Pliocene sea surface temperature gradient in the North Atlantic. *Paleoceanography and Paleoclimatology* **35**, e2020PA003905 (2020).
16. Naafs, B., Hefter, J. & Stein, R. Millennial-scale ice rafting events and Hudson Strait Heinrich (-like) Events during the late Pliocene and Pleistocene: a review. *Quaternary Science Reviews* **80**, 1–28 (2013).
17. Voelker, A. H. & Abreu, L. d. A review of abrupt climate change events in the Northeastern Atlantic Ocean (Iberian Margin): latitudinal, longitudinal and vertical gradients. *AGU Geophysical Monograph* (2010).
18. de Abreu, L., Shackleton, N. J., Schönfeld, J., Hall, M. & Chapman, M. Millennial-scale oceanic climate variability off the Western Iberian margin during the last two glacial periods. *Marine Geology* **196**, 1–20 (2003).
19. Salgueiro, E. *et al.* Past circulation along the western Iberian margin: a time slice vision from the Last Glacial to the Holocene. *Quaternary Science Reviews* **106**, 316–329 (2014).
20. Hodell, D. *et al.* Response of Iberian Margin sediments to orbital and suborbital forcing over the past 420 ka. *Paleoceanography* **28**, 185–199 (2013).
21. Martrat, B. *et al.* Four climate cycles of recurring deep and surface water destabilizations on the Iberian margin. *Science* **317**, 502–507 (2007).
22. Shackleton, N. J., Hall, M. A. & Vincent, E. Phase relationships between millennial-scale events 64,000–24,000 years ago. *Paleoceanography* **15**, 565–569 (2000).
23. Hodell, D. *et al.* A reference time scale for Site U1385 (Shackleton Site) on the SW Iberian Margin. *Global and Planetary Change* **133**, 49–64 (2015).

24. Bahr, A. *et al.* Oceanic heat pulses fueling moisture transport towards continental Europe across the mid-Pleistocene transition. *Quaternary Science Reviews* **179**, 48–58 (2018).

25. Voelker, A. H. *et al.* Mediterranean outflow strengthening during northern hemisphere coolings: a salt source for the glacial Atlantic? *Earth and Planetary Science Letters* **245**, 39–55 (2006).

26. Beuscher, S. *et al.* End-member modelling as a tool for climate reconstruction—an Eastern Mediterranean case study. *PLoS One* **12**, e0185136 (2017).

27. Ehrmann, W. & Schmiedl, G. Nature and dynamics of North African humid and dry periods during the last 200,000 years documented in the clay fraction of Eastern Mediterranean deep-sea sediments. *Quaternary Science Reviews* **260**, 106925 (2021).

28. Weldeab, S., Emeis, K.-C., Hemleben, C., Schmiedl, G. & Schulz, H. Spatial productivity variations during formation of sapropels S5 and S6 in the Mediterranean Sea: evidence from Ba contents. *Palaeogeography, Palaeoclimatology, Palaeoecology* **191**, 169–190 (2003).

29. Hendy, I. L., Kennett, J. P., Roark, E. & Ingram, B. L. Apparent synchroneity of submillennial scale climate events between Greenland and Santa Barbara Basin, California from 30–10 ka. *Quaternary Science Reviews* **21**, 1167–1184 (2002).

30. Hendy, I. L. & Kennett, J. P. Latest Quaternary North Pacific surface-water responses imply atmosphere-driven climate instability. *Geology* **27**, 291–294 (1999).

31. Hendy, I. L. & Kennett, J. P. Tropical forcing of North Pacific intermediate water distribution during Late Quaternary rapid climate change? *Quaternary Science Reviews* **22**, 673–689 (2003).

32. Clemens, S. *et al.* Precession-band variance missing from East Asian monsoon runoff. *Nature Communications* **9**, 1–12 (2018).

33. Nürnberg, D., Ziegler, M., Karas, C., Tiedemann, R. & Schmidt, M. W. Interacting Loop Current variability and Mississippi River discharge over the past 400 kyr. *Earth and Planetary Science Letters* **272**, 278–289 (2008).

34. Pichevin, L., Bard, E., Martinez, P. & Billy, I. Evidence of ventilation changes in the Arabian Sea during the late Quaternary: Implication for denitrification and nitrous oxide emission. *Global Biogeochemical Cycles* **21** (2007).

35. Schulz, H., von Rad, U. & Erlenkeuser, H. Correlation between Arabian Sea and Greenland climate oscillations of the past 110,000 years. *Nature* **393**, 54–57 (1998).

36. Deplazes, G. *et al.* Links between tropical rainfall and North Atlantic climate during the last glacial period. *Nature Geoscience* **6**, 213–217 (2013).

37. Deplazes, G. *et al.* Weakening and strengthening of the Indian monsoon during Heinrich events and Dansgaard-Oeschger oscillations. *Paleoceanography* **29**, 99–114 (2014).

38. Zhao, M., Beveridge, N., Shackleton, N., Sarnthein, M. & Eglinton, G. Molecular stratigraphy of cores off northwest Africa: Sea surface temperature history over the last 80 ka. *Paleoceanography* **10**, 661–675 (1995).

39. Lauterbach, S. *et al.* An ~130 kyr record of surface water temperature and δ18O from the northern Bay of Bengal: Investigating the linkage between Heinrich events and Weak Monsoon Intervals in Asia. *Paleoceanography and Paleoclimatology* **35**, e2019PA003646 (2020).

40. Clemens, S. C. *et al.* Remote and local drivers of Pleistocene South Asian summer monsoon precipitation: A test for future predictions. *Science Advances* **7**, eabg3848 (2021).

41. Zarriess, M. & Mackensen, A. The tropical rainbelt and productivity changes off northwest Africa: A 31,000-year high-resolution record. *Marine Micropaleontology* **76**, 76–91 (2010).

42. Zarriess, M. *et al.* Bipolar seesaw in the northeastern tropical atlantic during heinrich stadials. *Geophysical Research Letters* **38** (2011).

43. Jung, S. J., Kroon, D., Ganssen, G., Peeters, F. & Ganeshram, R. Enhanced Arabian Sea intermediate water flow during glacial North Atlantic cold phases. *Earth and Planetary Science Letters* **280**, 220–228 (2009).

44. Rosenthal, Y., Oppo, D. W. & Linsley, B. K. The amplitude and phasing of climate change during the last deglaciation in the Sulu Sea, western equatorial Pacific. *Geophysical Research Letters* **30** (2003).

45. Stott, L., Poulsen, C., Lund, S. & Thunell, R. Super ENSO and global climate oscillations at millennial time scales. *Science* **297**, 222–226 (2002).

46. Saikku, R., Stott, L. & Thunell, R. A bi-polar signal recorded in the western tropical Pacific: Northern and Southern Hemisphere climate records from the Pacific warm pool during the last Ice Age. *Quaternary Science Reviews* **28**, 2374–2385 (2009).

47. Weldeab, S., Lea, D. W., Schneider, R. R. & Andersen, N. 155,000 years of West African monsoon and ocean thermal evolution. *Science* **316**, 1303–1307 (2007).

48. Lea, D. W. *et al.* Paleoclimate history of Galápagos surface waters over the last 135,000 yr. *Quaternary Science Reviews* **25**, 1152–1167 (2006).

49. Mohtadi, M. *et al.* North Atlantic forcing of tropical Indian Ocean climate. *Nature* **509**, 76–80 (2014).

50. Weijers, J. W., Schouten, S., Schefuß, E., Schneider, R. R. & Damste, J. S. S. Disentangling marine, soil and plant organic carbon contributions to continental margin sediments: a multi-proxy approach in a 20,000 year sediment record from the Congo deep-sea fan. *Geochimica et Cosmochimica Acta* **73**, 119–132 (2009).

51. Rampen, S. W. *et al.* Long chain 1, 13-and 1, 15-diols as a potential proxy for palaeotemperature reconstruction. *Geochimica et Cosmochimica Acta* **84**, 204–216 (2012).

52. De Pol-Holz, R. *et al.* Late Quaternary variability of sedimentary nitrogen isotopes in the eastern South Pacific Ocean. *Paleoceanography* **22** (2007).

53. De Deckker, P. *et al.* Climatic evolution in the Australian region over the last 94 ka-spanning human occupancy-, and unveiling the Last Glacial Maximum. *Quaternary Science Reviews* **249**, 106593 (2020).

54. Hodell, D. A., Venz, K. A., Charles, C. D. & Ninnemann, U. S. Pleistocene vertical carbon isotope and carbonate gradients in the South Atlantic sector of the Southern Ocean. *Geochemistry, Geophysics, Geosystems* **4**, 1–19 (2003).

55. Barker, S. & Diz, P. Timing of the descent into the last Ice Age determined by the bipolar seesaw. *Paleoceanography* **29**, 489–507 (2014).

56. Ziegler, M., Diz, P., Hall, I. R. & Zahn, R. Millennial-scale changes in atmospheric CO2 levels linked to the Southern Ocean carbon isotope gradient and dust flux. *Nature Geoscience* **6**, 457–461 (2013).

57. Elderfield, H. *et al.* Evolution of ocean temperature and ice volume through the mid-Pleistocene climate transition. *Science* **337**, 704–709 (2012).

58. Gottschalk, J., Skinner, L. C. & Waelbroeck, C. Contribution of seasonal sub-Antarctic surface water variability to millennial-scale changes in atmospheric CO2 over the last deglaciation and Marine Isotope Stage 3. *Earth and Planetary Science Letters* **411**, 87–99 (2015).

59. Riveiros, N. V. *et al.* Response of South Atlantic deep waters to deglacial warming during Terminations V and I. *Earth and Planetary Science Letters* **298**, 323–333 (2010).

60. Pahnke, K., Zahn, R., Elderfield, H. & Schulz, M. 340,000-year centennial-scale marine record of Southern Hemisphere climatic oscillation. *Science* **301**, 948–952 (2003).

61. Rickaby, R. E. M. & Elderfield, H. Planktonic foraminiferal Cd/Ca: paleonutrients or paleotemperature? *Paleoceanography* **14**, 293–303 (1999).

62. Westerhold, T. *et al.* An astronomically dated record of Earth's climate and its predictability over the last 66 million years. *Science* **369**, 1383–1387 (2020).

63. Rasmussen, S. O. *et al.* A first chronology for the North Greenland Eemian Ice Drilling (NEEM) ice core. *Climate of the Past* **9**, 2713–2730 (2013).

64. Erhardt, T. *et al.* Decadal-scale progression of the onset of Dansgaard–Oeschger warming events. *Climate of the Past* **15**, 811–825 (2019).

65. Gkinis, V. *et al.* A 120,000-year long climate record from a NW-Greenland deep ice core at ultra-high resolution. *Scientific Data* **8**, 1–9 (2021).

66. Rasmussen, S. O. *et al.* A stratigraphic framework for abrupt climatic changes during the Last Glacial period based on three synchronized Greenland ice-core records: refining and extending the INTIMATE event stratigraphy. *Quaternary Science Reviews* **106**, 14–28 (2014).

67. Baumgartner, M. *et al.* NGRIP CH 4 concentration from 120 to 10 kyr before present and its relation to a δ 15 N temperature reconstruction from the same ice core. *Climate of the Past* **10**, 903–920 (2014).

68. Thompson, L. G. *et al.* Tropical climate instability: The last glacial cycle from a Qinghai-Tibetan ice core. *Science* **276**, 1821–1825 (1997).

69. Bazin, L. *et al.* An optimized multi-proxy, multi-site Antarctic ice and gas orbital chronology (AICC2012): 120–800 ka. *Climate of the Past* **9**, 1715–1731 (2013).

70. Vallelonga, P. *et al.* Iron fluxes to Talos Dome, Antarctica, over the past 200 kyr. *Climate of the Past* **9**, 597–604 (2013).

71. Barbante, C. *et al.* One-to-one coupling of glacial climate variability in Greenland and Antarctica. *Nature* **444**, 195–198 (2006).

72. Jouzel, J. *et al.* Orbital and millennial Antarctic climate variability over the past 800,000 years. *Science* **317**, 793–796 (2007).

73. Lüthi, D. *et al.* High-resolution carbon dioxide concentration record 650,000–800,000 years before present. *Nature* **453**, 379–382 (2008).

74. Loulergue, L. *et al.* Orbital and millennial-scale features of atmospheric CH4 over the past 800,000 years. *Nature* **453**, 383–386 (2008).

75. Lambert, F. *et al.* Dust-climate couplings over the past 800,000 years from the EPICA Dome C ice core. *Nature* **452**, 616–619 (2008).

76. Extier, T. *et al.* On the use of δ18Oatm for ice core dating. *Quaternary Science Reviews* **185**, 244–257 (2018).

77. Lambert, F., Bigler, M., Steffensen, J. P., Hutterli, M. & Fischer, H. Centennial mineral dust variability in high-resolution ice core data from Dome C, Antarctica. *Climate of the Past* **8**, 609–623 (2012).

78. Uemura, R. *et al.* Asynchrony between Antarctic temperature and CO2 associated with obliquity over the past 720,000 years. *Nature Communications* **9**, 1–11 (2018).

79. Petit, J.-R. *et al.* Climate and atmospheric history of the past 420,000 years from the Vostok ice core, Antarctica. *Nature* **399**, 429–436 (1999).

80. WAIS Divide Project Members. Precise interpolar phasing of abrupt climate change during the last ice age. *Nature* **520**, 661–665 (2015).

81. Barker, S. *et al.* 800,000 years of abrupt climate variability. *Science* **334**, 347–351 (2011).

82. Moseley, G. E. *et al.* NALPS19: sub-orbital-scale climate variability recorded in northern Alpine speleothems during the last glacial period. *Climate of the Past* **16**, 29–50 (2020).

83. Boch, R. *et al.* NALPS: a precisely dated European climate record 120–60 ka. *Climate of the Past* **7**, 1247–1259 (2011).

84. Genty, D. *et al.* Precise dating of Dansgaard–Oeschger climate oscillations in western Europe from stalagmite data. *Nature* **421**, 833–837 (2003).

85. Genty, D. *et al.* Isotopic characterization of rapid climatic events during OIS3 and OIS4 in Villars Cave stalagmites (SW-France) and correlation with Atlantic and Mediterranean pollen records. *Quaternary Science Reviews* **29**, 2799–2820 (2010).

86. Cheng, H. *et al.* The climatic cyclicity in semiarid-arid central Asia over the past 500,000 years. *Geophysical Research Letters* **39** (2012).

87. Fleitmann, D. *et al.* Timing and climatic impact of Greenland interstadials recorded in stalagmites from northern Turkey. *Geophysical Research Letters* **36** (2009).

88. Cheng, H. *et al.* Climate variations of Central Asia on orbital to millennial timescales. *Scientific Reports* **6**, 1–11 (2016).

89. Lachniet, M. S., Denniston, R. F., Asmerom, Y. & Polyak, V. J. Orbital control of western North America atmospheric circulation and climate over two glacial cycles. *Nature Communications* **5**, 1–8 (2014).

90. Ünal-İmer, E. *et al.* An 80 kyr-long continuous speleothem record from Dim Cave, SW Turkey with paleoclimatic implications for the Eastern Mediterranean. *Scientific Reports* **5**, 1–11 (2015).

91. Moseley, G. E. *et al.* Reconciliation of the Devils Hole climate record with orbital forcing. *Science* **351**, 165–168 (2016).

92. Asmerom, Y., Polyak, V. J. & Burns, S. J. Variable winter moisture in the southwestern United States linked to rapid glacial climate shifts. *Nature Geoscience* **3**, 114–117 (2010).

93. Wang, Y.-J. *et al.* A high-resolution absolute-dated late Pleistocene monsoon record from Hulu Cave, China. *Science* **294**, 2345–2348 (2001).

94. Wagner, J. D. *et al.* Moisture variability in the southwestern United States linked to abrupt glacial climate change. *Nature Geoscience* **3**, 110–113 (2010).

95. Wang, Y. *et al.* Millennial-and orbital-scale changes in the East Asian monsoon over the past 224,000 years. *Nature* **451**, 1090–1093 (2008).

96. Cheng, H. *et al.* The Asian monsoon over the past 640,000 years and ice age terminations. *Nature* **534**, 640–646 (2016).

97. Bar-Matthews, M., Ayalon, A., Gilmour, M., Matthews, A. & Hawkesworth, C. J. Sea–land oxygen isotopic relationships from planktonic foraminifera and speleothems in the Eastern Mediterranean region and their implication for paleorainfall during interglacial intervals. *Geochimica et Cosmochimica Acta* **67**, 3181–3199 (2003).

98. Kathayat, G. *et al.* Indian monsoon variability on millennial-orbital timescales. *Scientific Reports* **6**, 1–7 (2016).

99. Arienzo, M. M. *et al.* Bahamian speleothem reveals temperature decrease associated with Heinrich stadials. *Earth and Planetary Science Letters* **430**, 377–386 (2015).

100. Kelly, M. J. *et al.* High resolution characterization of the Asian Monsoon between 146,000 and 99,000 years BP from Dongge Cave, China and global correlation of events surrounding Termination II. *Palaeogeography, Palaeoclimatology, Palaeoecology* **236**, 20–38 (2006).

101. Burns, S. J., Fleitmann, D., Matter, A., Kramers, J. & Al-Subbary, A. A. Indian Ocean climate and an absolute chronology over Dansgaard/Oeschger events 9 to 13. *Science* **301**, 1365–1367 (2003).

102. Lachniet, M. S. *et al.* Late Quaternary moisture export across Central America and to Greenland: evidence for tropical rainfall variability from Costa Rican stalagmites. *Quaternary Science Reviews* **28**, 3348–3360 (2009).

103. Carolin, S. A. *et al.* Varied response of western Pacific hydrology to climate forcings over the last glacial period. *Science* **340**, 1564–1566 (2013).

104. Mosblech, N. A. *et al.* North Atlantic forcing of Amazonian precipitation during the last ice age. *Nature Geoscience* **5**, 817–820 (2012).

105. Wang, X. *et al.* Hydroclimate changes across the Amazon lowlands over the past 45,000 years. *Nature* **541**, 204–207 (2017).

106. Kanner, L. C., Burns, S. J., Cheng, H. & Edwards, R. L. High-latitude forcing of the South American summer monsoon during the last glacial. *Science* **335**, 570–573 (2012).

107. Stríkis, N. M. *et al.* South American monsoon response to iceberg discharge in the North Atlantic. *Proceedings of the National Academy of Sciences* **115**, 3788–3793 (2018).

108. Denniston, R. F. *et al.* North Atlantic forcing of millennial-scale Indo-Australian monsoon dynamics during the Last Glacial period. *Quaternary Science Reviews* **72**, 159–168 (2013).

109. Cruz, F. W. *et al.* Insolation-driven changes in atmospheric circulation over the past 116,000 years in subtropical Brazil. *Nature* **434**, 63–66 (2005).

110. Whittaker, T. E., Hendy, C. H. & Hellstrom, J. C. Abrupt millennial-scale changes in intensity of Southern Hemisphere westerly winds during marine isotope stages 2–4. *Geology* **39**, 455–458 (2011).

111. Seelos, K., Sirocko, F. & Dietrich, S. A continuous high-resolution dust record for the reconstruction of wind systems in central Europe (Eifel, Western Germany) over the past 133 ka. *Geophysical Research Letters* **36** (2009).

112. Rousseau, D.-D. *et al.* (MIS3 & 2) millennial oscillations in Greenland dust and Eurasian aeolian records–A paleosol perspective. *Quaternary Science Reviews* **169**, 99–113 (2017).

113. Moine, O. *et al.* The impact of Last Glacial climate variability in west-European loess revealed by radiocarbon dating of fossil earthworm granules. *Proceedings of the National Academy of Sciences* **114**, 6209–6214 (2017).

114. Újvári, G. *et al.* AMS 14C and OSL/IRSL dating of the Dunaszekcső loess sequence (Hungary): chronology for 20 to 150 ka and implications for establishing reliable age–depth models for the last 40 ka. *Quaternary Science Reviews* **106**, 140–154 (2014).

115. Sun, Y. *et al.* Influence of Atlantic meridional overturning circulation on the East Asian winter monsoon. *Nature Geoscience* **5**, 46–49 (2012).

116. Sun, Y. *et al.* Astronomical and glacial forcing of East Asian summer monsoon variability. *Quaternary Science Reviews* **115**, 132–142 (2015).

117. Sun, Y. *et al.* High-sedimentation-rate loess records: A new window into understanding orbital-and millennial-scale monsoon variability. *Earth-Science Reviews* **220**, 103731 (2021).

118. Yang, S. & Ding, Z. A 249 kyr stack of eight loess grain size records from northern China documenting millennial-scale climate variability. *Geochemistry, Geophysics, Geosystems* **15**, 798–814 (2014).

119. Sun, Y., Wang, X., Liu, Q. & Clemens, S. C. Impacts of post-depositional processes on rapid monsoon signals recorded by the last glacial loess deposits of northern China. *Earth and Planetary Science Letters* **289**, 171–179 (2010).

120. Hao, Q. *et al.* Delayed build-up of Arctic ice sheets during 400,000-year minima in insolation variability. *Nature* **490**, 393–396 (2012).

121. Sun, Y., Clemens, S. C., An, Z. & Yu, Z. Astronomical timescale and palaeoclimatic implication of stacked 3.6-myr monsoon records from the chinese loess plateau. *Quaternary Science Reviews* **25**, 33–48 (2006).

122. Ding, Z. L. *et al.* Stacked 2.6-Ma grain size record from the Chinese loess based on five sections and correlation with the deep-sea δ18O record. *Paleoceanography* **17**, 5–1 (2002).

123. Melles, M. *et al.* 2.8 million years of Arctic climate change from Lake El'gygytgyn, NE Russia. *Science* **337**, 315–320 (2012).

124. Meyer-Jacob, C. *et al.* Biogeochemical variability during the past 3.6 million years recorded by FTIR spectroscopy in the sediment record of Lake El'gygytgyn, Far East Russian Arctic. *Climate of the Past* **10**, 209–220 (2014).

125. Prokopenko, A. A., Hinnov, L. A., Williams, D. F. & Kuzmin, M. I. Orbital forcing of continental climate during the Pleistocene: a complete astronomically tuned climatic record from Lake Baikal, SE Siberia. *Quaternary Science Reviews* **25**, 3431–3457 (2006).

126. Müller, U. C., Pross, J. & Bibus, E. Vegetation response to rapid climate change in Central Europe during the past 140,000 yr based on evidence from the Füramoos pollen record. *Quaternary Research* **59**, 235–245 (2003).

127. Ampel, L., Wohlfarth, B., Risberg, J. & Veres, D. Paleolimnological response to millennial and centennial scale climate variability during MIS 3 and 2 as suggested by the diatom record in Les Echets, France. *Quaternary Science Reviews* **27**, 1493–1504 (2008).

128. Veres, D. *et al.* Climate-driven changes in lake conditions during late MIS 3 and MIS 2: a high-resolution geochemical record from Les Echets, France. *Boreas* **38**, 230–243 (2009).

129. Reille, M. & De Beaulieu, J. Pollen analysis of a long upper Pleistocene continental sequence in a Velay maar (Massif Central, France). *Palaeogeography, Palaeoclimatology, Palaeoecology* **80**, 35–48 (1990).

130. Benson, L., Lund, S., Negrini, R., Linsley, B. & Zic, M. Response of north American Great basin lakes to Dansgaard–Oeschger oscillations. *Quaternary Science Reviews* **22**, 2239–2251 (2003).

131. Follieri, M., Magri, D. & Sadori, L. Pollen stratigraphical synthesis from Valle di Castiglione (Roma). *Quaternary International* **3**, 81–84 (1989).

132. Tzedakis, P., Hooghiemstra, H. & Pälike, H. The last 1.35 million years at Tenaghi Philippon: revised chronostratigraphy and long-term vegetation trends. *Quaternary Science Reviews* **25**, 3416–3430 (2006).

133. Wagner, B. *et al.* Mediterranean winter rainfall in phase with African monsoons during the past 1.36 million years. *Nature* **573**, 256–260 (2019).

134. Francke, A. *et al.* Sedimentological processes and environmental variability at Lake Ohrid (Macedonia, Albania) between 637 ka and the present. *Biogeosciences* **13**, 1179–1196 (2016).

135. Sadori, L. *et al.* Pollen-based paleoenvironmental and paleoclimatic change at Lake Ohrid (south-eastern Europe) during the past 500 ka. *Biogeosciences* **13**, 1423–1437 (2016).

136. Donders, T. *et al.* 1.36 million years of Mediterranean forest refugium dynamics in response to glacial–interglacial cycle strength. *Proceedings of the National Academy of Sciences* **118** (2021).

137. Allen, J. R. *et al.* Rapid environmental changes in southern Europe during the last glacial period. *Nature* **400**, 740–743 (1999).

138. Allen, J. R., Watts, W. A. & Huntley, B. Weichselian palynostratigraphy, palaeovegetation and palaeoenvironment; the record from Lago Grande di Monticchio, southern Italy. *Quaternary International* **73**, 91–110 (2000).

139. Huntley, B., Watts, W., Allen, J. & Zolitschka, B. Palaeoclimate, chronology and vegetation history of the Weichselian Lateglacial: comparative analysis of data from three cores at Lago Grande di Monticchio, southern Italy. *Quaternary Science Reviews* **18**, 945–960 (1999).

140. Tzedakis, P. *et al.* Ecological thresholds and patterns of millennial-scale climate variability: The response of vegetation in Greece during the last glacial period. *Geology* **32**, 109–112 (2004).

141. Pickarski, N. & Litt, T. A new high-resolution pollen sequence at Lake Van, Turkey: insights into penultimate interglacial–glacial climate change on vegetation history. *Climate of the Past* **13**, 689–710 (2017).

142. Camuera, J. *et al.* Orbital-scale environmental and climatic changes recorded in a new 200,000-year-long multiproxy sedimentary record from Padul, southern Iberian Peninsula. *Quaternary Science Reviews* **198**, 91–114 (2018).

143. Camuera, J. *et al.* Chronological control and centennial-scale climatic subdivisions of the Last Glacial Termination in the western Mediterranean region. *Quaternary Science Reviews* **255**, 106814 (2021).

144. Camuera, J. *et al.* Past 200 kyr hydroclimate variability in the western mediterranean and its connection to the african humid periods. *Scientific Reports* **12**, 1–13 (2022).

145. Miebach, A., Stolzenberger, S., Wacker, L., Hense, A. & Litt, T. A new Dead Sea pollen record reveals the last glacial paleoenvironment of the southern Levant. *Quaternary Science Reviews* **214**, 98–116 (2019).

146. Grimm, E. C. *et al.* Evidence for warm wet Heinrich events in Florida. *Quaternary Science Reviews* **25**, 2197–2211 (2006).

147. Tierney, J. E. *et al.* Northern hemisphere controls on tropical southeast African climate during the past 60,000 years. *Science* **322**, 252–255 (2008).

148. Johnson, T. C. *et al.* A progressively wetter climate in southern East Africa over the past 1.3 million years. *Nature* **537**, 220–224 (2016).

149. Fritz, S. C. *et al.* Quaternary glaciation and hydrologic variation in the South American tropics as reconstructed from the Lake Titicaca drilling project. *Quaternary Research* **68**, 410–420 (2007).

150. Fritz, S. C., Baker, P., Ekdahl, E., Seltzer, G. & Stevens, L. Millennial-scale climate variability during the Last Glacial period in the tropical Andes. *Quaternary Science Reviews* **29**, 1017–1024 (2010).

151. Bagniewski, W., Ghil, M. & Rousseau, D.-D. Automatic detection of abrupt transitions in paleoclimate records. *Chaos* **31**, 113129 (2021).

152. Rousseau, D.-D., Bagniewski, W. & Ghil, M. Abrupt climate changes and the astronomical theory: are they related? *Climate of the Past* **18**, 249–271 (2022).